

**GRAVITY RULES OVER PHOTONS IN THE GREENHOUSE EFFECT:
Convection Controls the Energy Transfer through the Troposphere and Pressure
Broadening Controls the LWIR Emission to Space**

Roy Clark

SUMMARY

When the atmospheric energy transfer processes related to the ‘greenhouse effect’ are examined in detail it becomes very clear that gravity controls the LWIR photon emission to space through convection and pressure broadening. The ground temperature is set by the short term dynamic energy balance of the surface flux. This can vary from +1000 to -100 W.m⁻² during the day. There can be no equilibrium. The small ‘clear sky’ increase of 1.7 W.m⁻² in the downward atmospheric LWIR flux from a 100 ppm increase in atmospheric CO₂ concentration over 200 years has to be added to the total flux coupled dynamically to the surface. The total cumulative flux from 1.7 W.m⁻² is 0.15 MJ.m⁻² per day. This is equivalent to about 2.5 minutes of full summer sun at 1000 W.m⁻² or the daily evaporation of a film of water 65 micron thick over an area of 1 m². It is impossible for a 100 ppm increase in atmospheric CO₂ concentration to have any measurable effect on the ground temperature or the meteorological surface air temperature measured 1.5 to 2 m above the ground. The greenhouse effect has to be described in terms of a daily ‘impulse’ of convective energy rising through the atmosphere that is produced by the solar heating of the surface. This ‘resets’ the lapse rate on a daily basis depending on the local weather conditions. The downward LWIR flux near the surface is determined by the ‘effective’ air temperature near the ground. Most of this downward atmospheric flux originates from within the first kilometer air layer above the surface. The Kirchoff exchange of this flux with the surface reduces the surface radiation emitted to space, but the air temperature is determined by the daily convection and the local weather system, not by ‘greenhouse gas absorption’. In the lower troposphere the emission from molecular lines is sufficiently pressure broadened that the downward LWIR flux within the atmospheric bands is close to that of a black body. The air temperature and the humidity set the width of the LWIR transmission window. Convection is a mass transport process. As the air rises through the atmosphere it has to overcome the Earth’s gravitational potential. Heat is converted to mechanical work and the air cools. The thermal energy that is not used in the upward convective expansion of the air through the atmosphere is radiated into space. This LWIR radiation is produced as a result of the transition from LWIR flux exchange to a free photon flux as molecular linewidths decrease with altitude. This process is dominated by H₂O because of the decrease in H₂O concentration with altitude as the vapor pressure decreases with temperature. Changes in CO₂ concentration of 100 ppm have no effect on the overall process of energy transfer from the surface. This is controlled by gravity through convection and molecular line narrowing, not by LWIR photons. Gravity rules the greenhouse effect through bulk thermodynamics. The resulting temperature and pressure profile – the lapse rate – controls the LWIR photon emission to space from the troposphere.

1.0 Introduction

The concept that IR absorbing gases helped to warm the atmosphere ‘like heat trapped under a pane of glass’ was first introduced by Joseph Fourier in 1827.^[1] Starting in 1859, John Tyndall began his studies of the infra red absorption of gases and correctly identified water vapor, followed by carbon dioxide as the most important IR absorbing gases in the atmosphere.^[2] He was also interested in the study of glaciers and accepted the Ice Age glaciation theories of Louis Agassiz.^[3] This led him to propose that changes in CO₂ concentration might be responsible for climate change. This idea was resurrected by Svante Arrhenius in 1896.^[4] The first quantitative evidence for an increase in atmospheric CO₂ concentration was provided by Guy Stewart Callendar in 1938.^[5] The relationship between CO₂ in the atmosphere and its intake by the oceans was first quantified by Roger Revelle and Hans Suess in 1957.^[6] However, no direct quantitative relationship between changes in atmospheric CO₂ concentration and climate change has ever been established. This is because none exists. The empirical speculation over CO₂ and climate change that originated with John Tyndall has been perpetuated as pseudoscientific dogma. Physical reality has been ignored in favor of computer models that have been empirically ‘calibrated’ or rather ‘hard wired’ to produce global warming.^[7]

The basic idea underlying the ‘greenhouse effect’ is that the IR active ‘greenhouse’ gases in the atmosphere absorb radiation from the surface and re-radiate it. This couples the thermal radiation from the surface to the atmosphere and enables the atmosphere to act as a ‘blanket’ that keeps the surface warmer than it would otherwise be. The usual argument is based on a simple thermal equilibrium assumption that the surface ‘average equilibrium’ temperature is 288 K and that the ‘effective average’ atmospheric emission temperature is 255 K. This difference of 33 K is defined as the greenhouse effect temperature.^[8]

In reality, the energy transfer processes that set the Earth’s surface temperature are rather more complex than the simple thermal blanket description. The basic ideas of average equilibrium temperatures and fluxes must be set aside and the energy transfer must be considered from a dynamic energy balance perspective. The surface heating and cooling fluxes at the Earth’s surface are always changing. This means that the energy flux from the surface that is coupled into the atmosphere is always changing. There is no possibility of equilibrium. Furthermore, the dominant energy transfer process through the troposphere is convection, not radiation. As the air rises through the atmosphere it has to work against gravity. Therefore, the air expands and cools. The temperature profile in the troposphere is set by the bulk thermodynamics of the convection as measured by the lapse rate, not by ‘greenhouse gas absorption’. As the altitude increases, the pressure and the temperature decrease. The density profile of the atmosphere is set by gravity. The upward atmospheric pressure has to balance the downward force of the weight of the atmosphere above. The pressure in turn sets the linewidth of the individual absorption emission lines in the atmosphere through pressure broadening induced by molecular collisions.^[9] As the re-absorption of LWIR radiation in the wings of the molecular lines decreases at higher altitudes, there is a transition from Kirchoff exchange to the free LWIR flux that is emitted at the top of the atmosphere. Gravity rules the real ‘greenhouse effect’ through convection and molecular line broadening.

The solar radiation that is absorbed at the Earth's surface is converted into thermal energy. This is transferred from the surface to the atmosphere through a combination of LWIR absorption, convection and latent heat flux. The absorption of the surface LWIR flux by the atmosphere and the convection depend on the temperature difference or thermal gradient near the surface. The temperature difference and therefore the heat transfer vary continuously on both a daily and a seasonal time frame. Water evaporation also cools the surface and the latent heat of evaporation is subsequently released into the atmosphere when the water condenses, usually at altitudes above 1 km. The LWIR absorption also depends on the atmospheric composition, mainly the humidity and the aerosol content. The surface LWIR flux that is absorbed by the atmosphere and the latent heat flux that is released both contribute to the convective flux. At least 90% of the excess LWIR flux from the surface outside of the LWIR transmission window is absorbed by the atmospheric bands within the first kilometer. The latent heat release usually occurs through cloud formation above 1 km. The IR active molecules in the atmosphere also emit LWIR radiation. The downward LWIR flux from the atmosphere balances most of the upward LWIR radiation from the surface, so the net night time cooling flux from the surface is approximately 40 W.m^{-2} . This process is called Kirchoff exchange. When cloud effects and humidity variations are included, the net night time cooling flux typically varies from 0 to 100 W.m^{-2} . This LWIR cooling flux is emitted directly to space from the surface through the atmospheric LWIR window in the spectral region from ~ 800 to $\sim 1200 \text{ cm}^{-1}$ (~ 12.5 to $\sim 8 \text{ }\mu\text{m}$). The IR active molecules in the atmosphere also emit LWIR radiation to space. On average, sufficient long wave infrared (LWIR) radiation is emitted back into space by the surface and the atmosphere to balance the incoming solar radiation so that the Earth's climate remains stable. This is a 'dynamic' balance not a formal equilibrium process. The atmosphere is continuously cooling through the LWIR emission to space. The energy lost to space is replaced by a convective energy 'pulse' that is produced by the daily solar heating of the surface augmented by some direct solar heating of the atmosphere. The peak solar flux at the surface under full summer sun conditions is approximately 1000 W.m^{-2} . This corresponds to a blackbody emission temperature of 91.4 C . Convection and the rotation of the Earth prevent the land surface from reaching this temperature. The energy transfer processes at the Earth's air-ocean and air-land interfaces are different and need to be considered separately. Over the oceans, the solar flux can penetrate to depths of up to 100 m. The heated subsurface ocean layers are transported and re-circulated over long distances by ocean currents. The various energy transfer processes that need to be considered in the real or dynamic greenhouse effect are summarized in Figure 1.

The fundamental point that is not generally understood or is perhaps ignored in climate studies is that climate is set by long term changes in short term energy transfer fluctuations. Unless the short term fluctuations are explicitly addressed, it is not possible to reproduce the longer term trends. These short term energy transfer processes can be divided into five areas: the surface energy transfer at the air-ocean and the air-land interfaces, the downward LWIR flux from the atmosphere, the convective transport through the atmosphere and the LWIR emission to space. These will now be considered in turn.

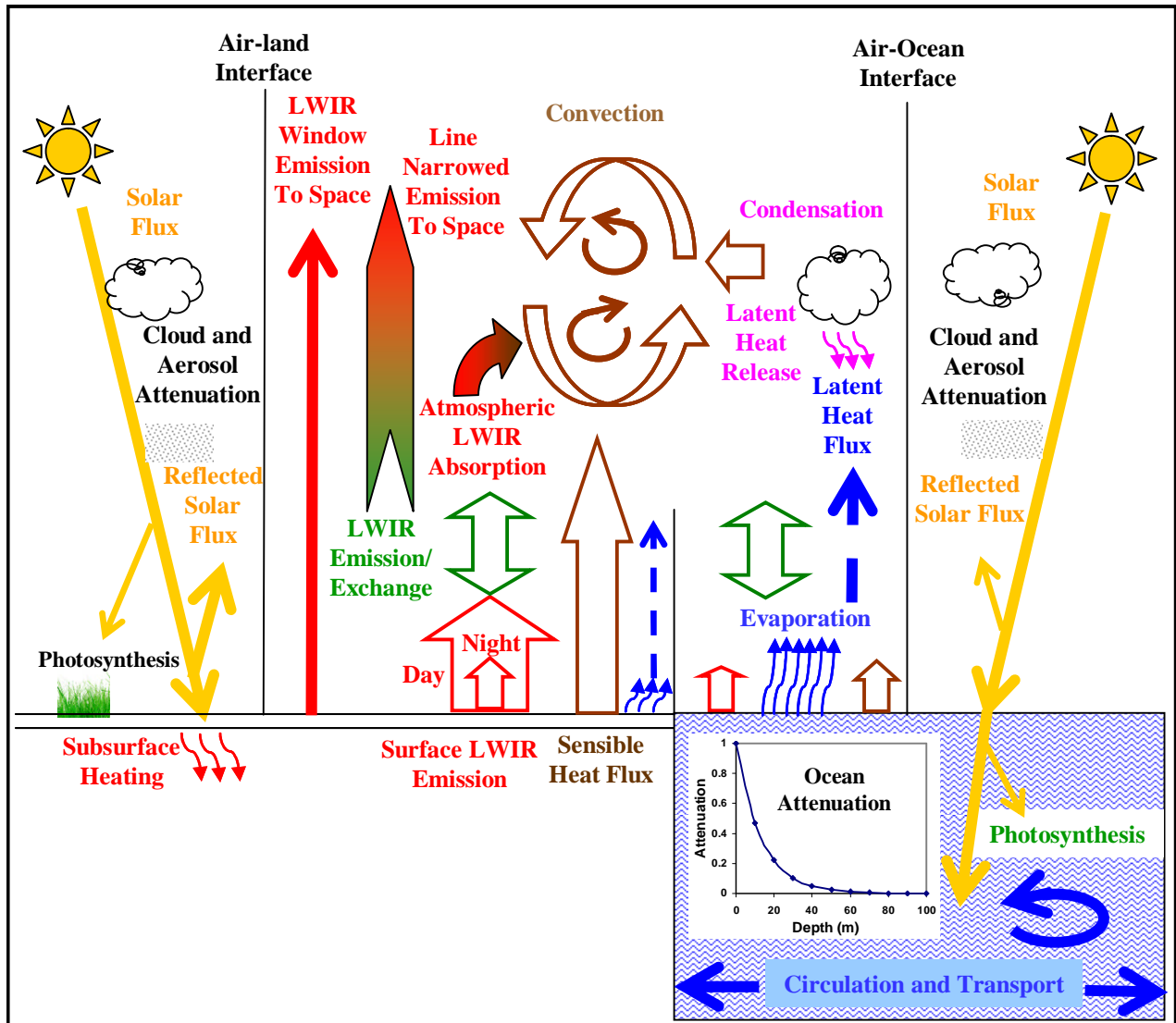


Figure 1: Surface energy transfer at the air-land and air-ocean interfaces (schematic).

2.0 The Air-Ocean Interface

Over the ocean, the solar radiation penetrates to depths of up to 100m. At the surface, the long term average surface air temperature is only ~ 2 K lower than the ocean surface temperature.^[10] The dominant energy transfer processes at most latitudes are evaporation and LWIR cooling through emission within the LWIR transmission window. Long term zonal averages of ocean temperature, energy flux, humidity and wind speed are presented in Figure 2.

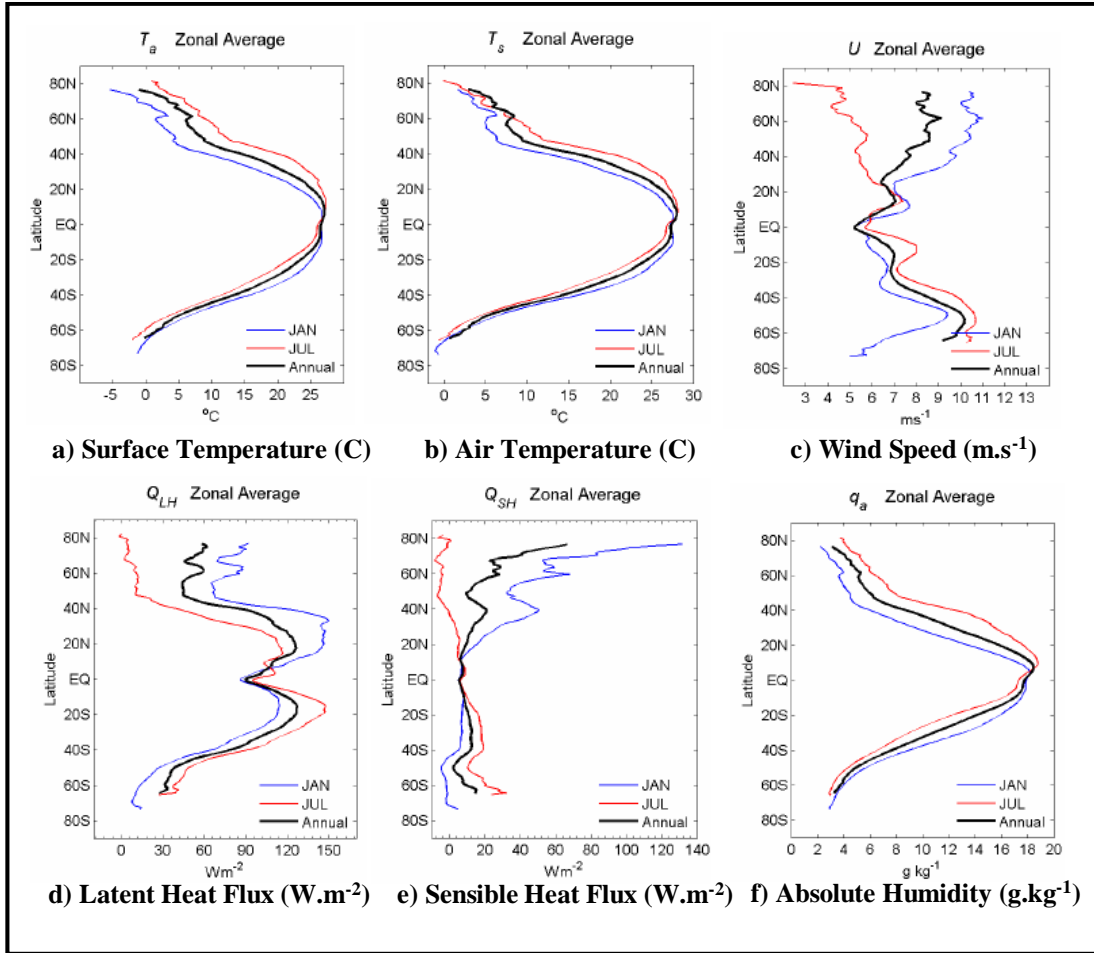


Figure 2: Long term, 50 year ocean zonal (latitude) averages. ^[10]

Historically, data on subsurface ocean temperatures has been very sparse. This has changed with the Argo Float Program. ^[11] There are now 3000 floats in the world's oceans that drift and record ocean temperature profiles and other data every 10 days. In general, as the sun warms the ocean during the spring and summer, a stable thermal gradient develops below a daily uniform mixing layer. During the fall and winter, cooling from the surface extends to lower depths and a uniform temperature layer forms that reaches to depths of 100 m or more. Figure 3 shows the 2007 annual profile data from two selected Argo floats located in the S. Central Pacific Ocean. One is near the equator with an average latitude of -1.5 deg. The other has an average latitude of -20.9 deg. ^[7] Near the equator, the daily mixing layer does not generally extend below 50 m. Therefore, subsurface ocean layers below 50 m near the equator can accumulate solar heat for extended periods. This is the origin of the ENSO cycles and related phenomena such as periodic fluctuations in hurricane intensity. These warm subsurface ocean layers can be transported and re-circulated over long distances by ocean currents and gyres without any interaction with the ocean surface. At higher latitudes, seasonal cooling mixes the ocean layers uniformly to depths below the 100 m solar heating region. The ocean has to cool to -1.8 C before ocean water can freeze.

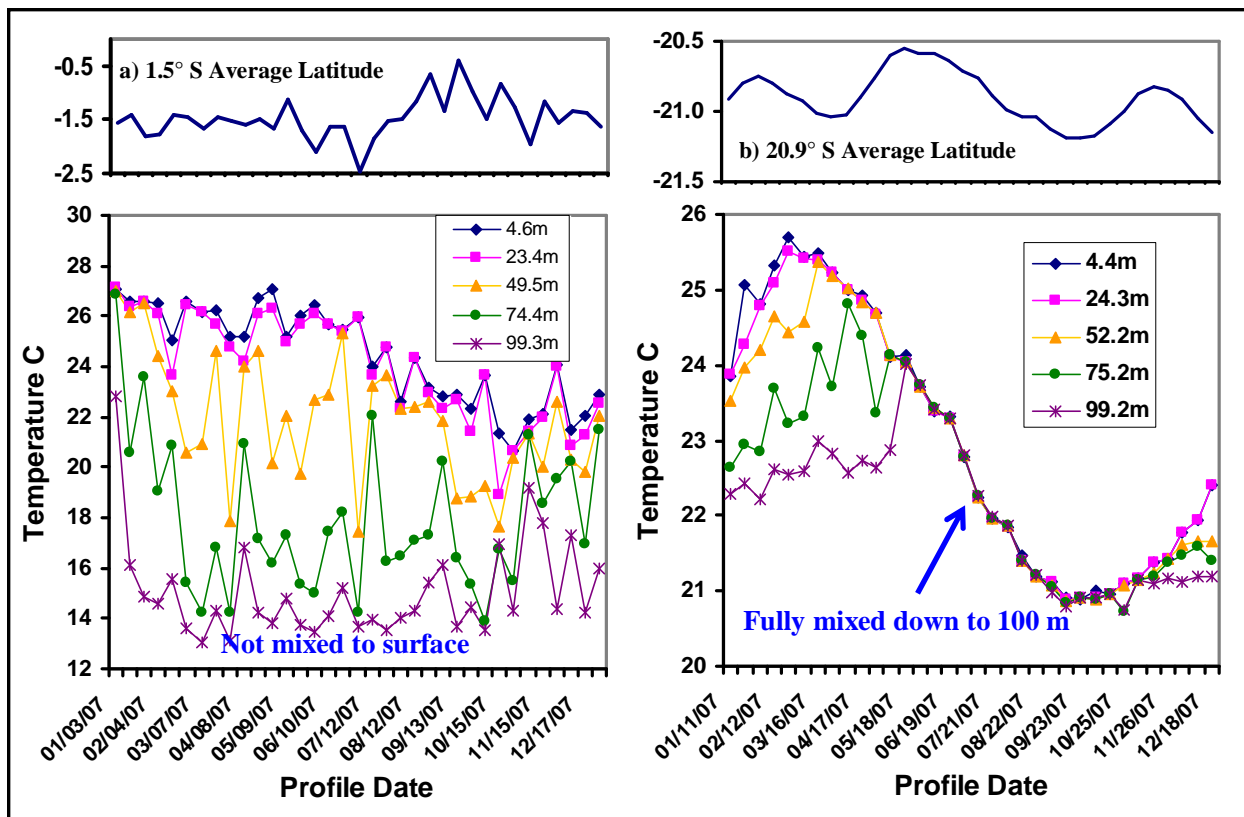


Figure 3: Argo float data from 2 floats in the central S. Pacific Ocean.

In contrast to solar heating, the penetration depth of the downward LWIR flux from the atmosphere into the ocean is less than 100 μm , about the width of a human hair. The penetration depth (99% attenuation) of visible and IR radiation into pure water is shown in Figure 4.^[12]

Small increases in LWIR emission from the atmosphere are converted into increases in ocean surface evaporation that are too small to detect in the wind driven fluctuations observed in such evaporation. Between 1977 and 2003, average ocean evaporation increased by 11 cm per year from 103 to 114 cm per year.^[13] This was caused by an increase in average wind speed of 0.1 meters per second. The uncertainty in the estimate was 2.7 cm per year which is larger than the upper 'clear sky' limit to the evaporation produced by a 100 ppm increase in CO_2 concentration over 200 years. This is illustrated in Figure 5. It is simply impossible for a 100 ppm increase in atmospheric CO_2 concentration to have any effect on ocean temperatures.

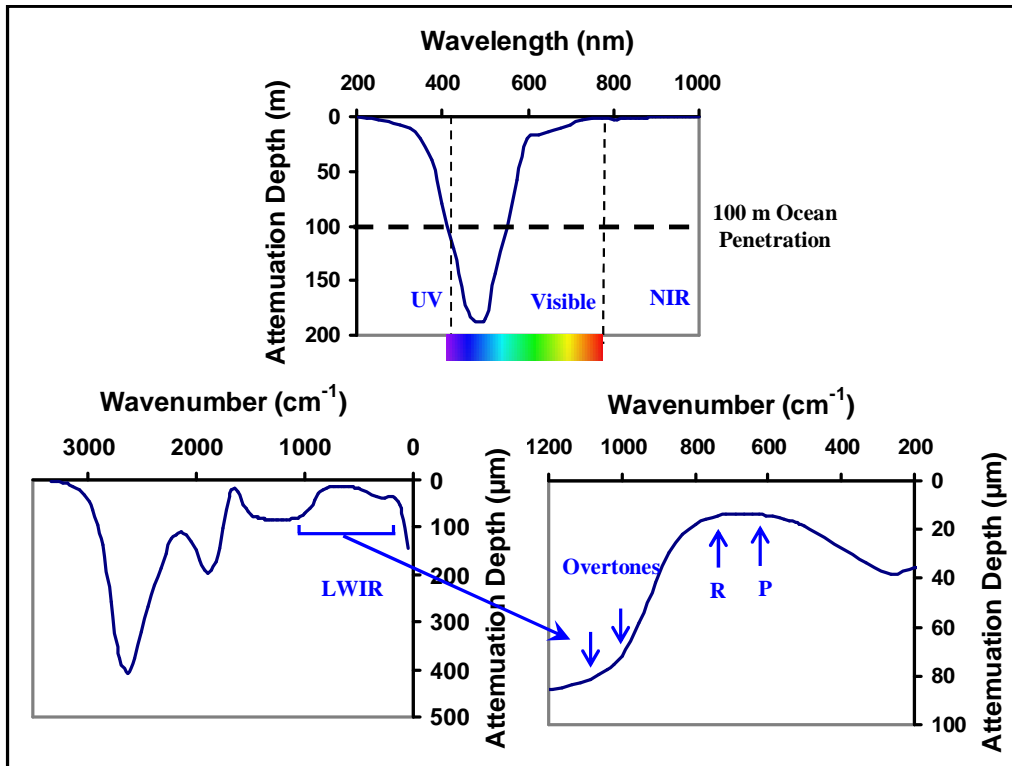


Figure 4: The attenuation depth of water in the visible and the LWIR spectral regions. Near 450 nm, solar radiation can penetrate up to 100 m into the ocean. In the LWIR region, the penetration depth of CO₂ radiation is less than 100 μm. The arrows indicate the location of the CO₂ emission bands. Please note the scale changes from meters to microns and nm to cm⁻¹. [12]

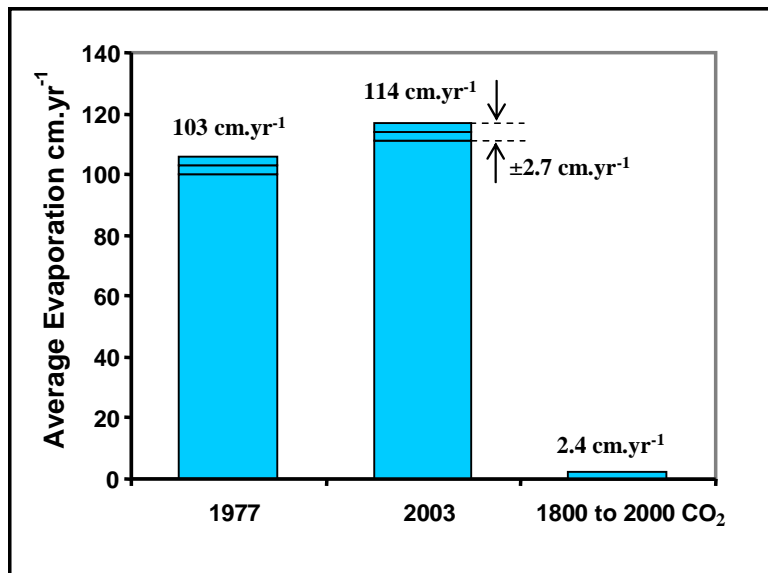


Figure 5: Average ocean evaporation increased from 103 to 114 cm.yr⁻¹ between 1977 and 2003 because of an increase in wind speed of 0.1 m.s⁻¹. [13] The uncertainty of 2.7 cm.yr⁻¹ was larger than the 'clear sky' upper limit to evaporation from a 1.7 W.m⁻² increase in LWIR flux caused by CO₂ over the last 200 years.

The Earth's weather patterns and therefore long term climate variations are set by ocean surface temperatures. These in turn are determined by the ability of the oceans cool through the transport of accumulated solar energy to the surface where cooling occurs mainly through LWIR emission and evaporation. This is a dynamic, non-equilibrium fluid transport process. Small changes in the solar constant, of the order of 1 W.m^{-2} or less are capable of causing climate change including the Ice Ages, the Maunder Minimum and the Medieval and recent ocean warming periods.^[7,14] The Earth's climate is set by an incident solar flux of $1365 \pm 1 \text{ W.m}^{-2}$. The increase of 1 W.m^{-2} corresponds to the short term increase in solar flux from the sunspot cycle.^[15] The decrease of 1 W.m^{-2} corresponds to the long term decrease in solar flux from Milankovitch cycles due to variations in the ellipticity of the Earth's orbit.^[16] Superimposed on the solar flux cycles are changes in ocean circulation that occur as the continents are shifted by plate tectonics. The most recent change in ocean circulation was the elevation of the Isthmus of Panama about 3 million years ago. Changes in the solar flux and ocean circulation are sufficient to explain most of the observed changes in the Earth's climate.^[17] Other effects include volcanic eruptions and meteor impacts. The observed changes in CO_2 concentration in the atmosphere are a response to changes in ocean temperatures. They are not a cause of climate change.

3.0 The Air-Land Interface

Over land, the solar energy is converted to thermal energy at the surface and energy storage is localized and limited to the first few meters below the surface. The dominant energy transfer processes for dry ground are convection and LWIR cooling. In addition, if the ground is moist, the latent heat flux may also be significant. The subsurface thermal storage varies on a daily and a seasonal time frame. The basic energy transfer processes at the air-ocean and air-land surfaces are illustrated above in Figure 1. The meteorological surface air temperature (MSAT) is the air temperature measured in an enclosure placed 1.5 to 2 m above the ground.^[18] There is no simple or obvious relationship between MSAT and actual surface temperature.

The ground surface temperature is set by the dynamic energy balance of the surface energy flux. This is usually dominated by convection and evaporation. The downward LWIR flux from the atmosphere exchanges LWIR flux with the surface. This helps to slow the cooling of the surface, particularly at night, but it is just one of several dynamic energy balance factors that determine the surface temperature. The change in surface energy balance and temperature during a 24 hour period for full summer sun conditions is illustrated in Figure 6. This is based on measured flux data from a micrometeorological station located in S. California.^[19] During the early morning hours, the surface is cooling predominantly by LWIR emission through the atmospheric LWIR window. During the day, the ground is heated by the solar flux. The ground cools through a combination of convection (sensible heat), evaporation (latent heat) and LWIR emission. The maximum ground temperature may easily exceed 50 C. Some of the surface heat is also conducted and stored below ground and released during the early evening hours. The maximum MSAT at 2 m elevation stays 20 C lower than the ground temperature. It is determined by the convective heating and air mixing near the surface. The 1.7 W.m^{-2} increase in downward LWIR flux from a 100 ppm increase in atmospheric CO_2 concentration can have no effect on the observed surface or air temperatures. The cumulative daily increase in LWIR flux from the 100 ppm increase in CO_2 is approximately 0.15 MJ.m^{-2} . This is equivalent to the daily

evaporation of a film of water 65 micron thick over a 1 m² area. Alternatively it is the cumulative flux of the sun shining at full intensity for 2.5 minutes. Once the increase in LWIR flux from a 100 ppm increase in atmospheric CO₂ concentration is correctly incorporated into the daily flux variation before averaging, the whole AGW argument disappears.

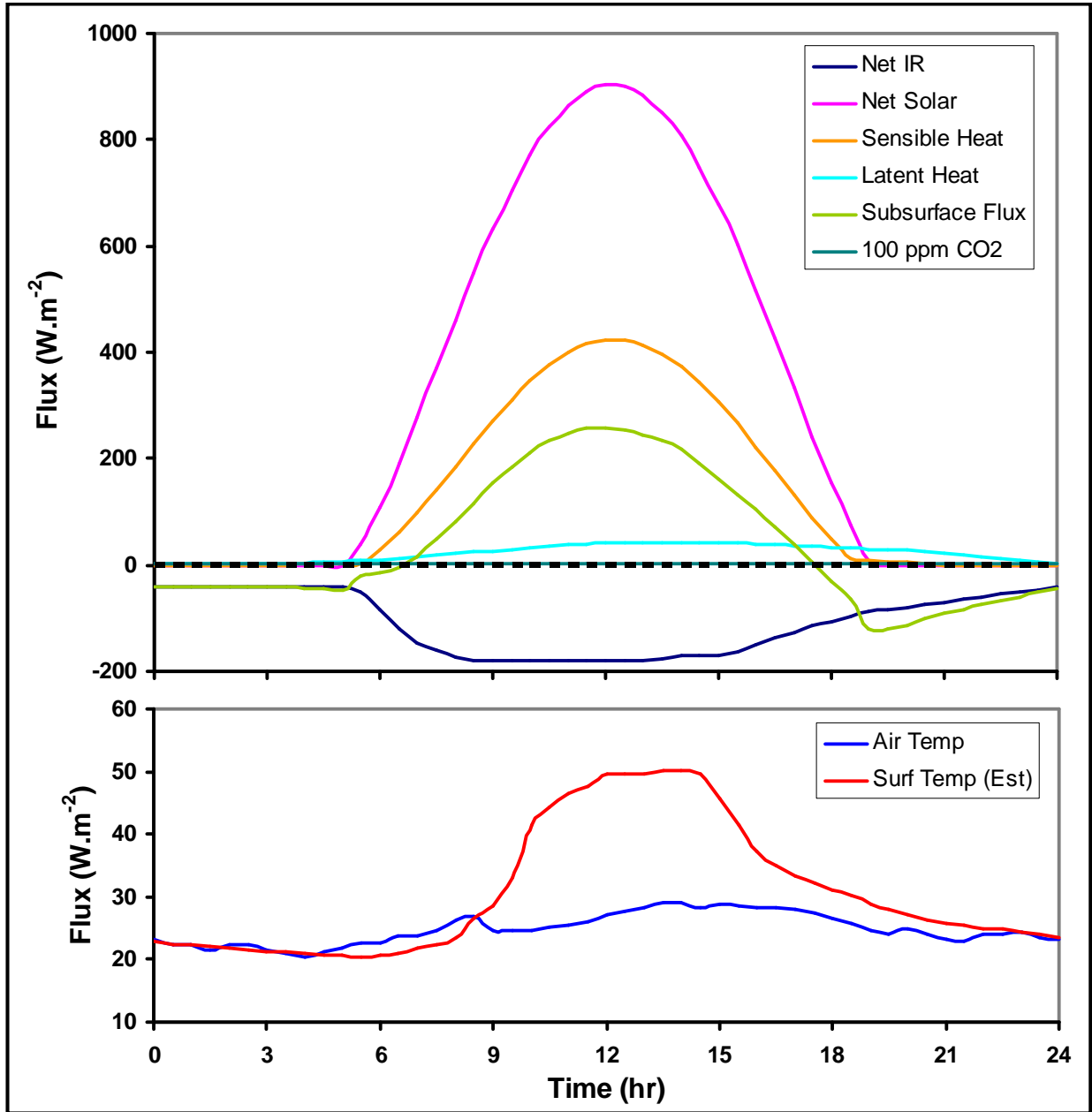


Figure 6: Approximate daily variation in surface flux terms and surface and air temperatures for full summer sun conditions. (Schematic: based on S. California data).^[19]

4.0 The Downward LWIR Flux at the Surface

The upward blackbody LWIR flux from the surface is balanced in large part by the downward flux from the atmosphere. This is a form of Kirchoff exchange energy, but there is no equilibrium. The upward flux from the surface depends on the ground surface temperature. The downward flux depends on the air temperature, the humidity and the cloud cover. The net upward 'clear sky' cooling flux at night from the surface is typically $\sim 40 \text{ W.m}^{-2}$. This is emitted directly to space through the LWIR atmospheric window. Under low humidity conditions, this cooling flux may increase to $\sim 100 \text{ W.m}^{-2}$. If low clouds are present, they may close the LWIR window completely and the net cooling flux will decrease to zero. In this case, the cloud base temperature matches the ground temperature. The effects of clouds are considered in more detail in Section 4.1 below.

Unless the humidity is low, at least 90% of the downward atmospheric flux reaching the surface originates within the first kilometer above the ground. It is also important to understand that the net heat required to maintain the temperature of the first km layer is usually a relatively small fraction of the total heat flux passing through the layer each day from surface convection. The heat capacity of a 1 m^2 column of air in the first kilometer layer is $\sim 1.2 \text{ MJ}$. Convection slows at night as the air and ground temperatures reach similar values. The air then cools predominantly through radiative emission. Since the thermal gradients are small, often less than 10 K.km^{-1} , the radiative emission rate within the atmospheric IR bands is approximately $50 \text{ W.m}^{-2}.\text{km}^{-1}$ for 'clear sky' conditions with moderate humidity levels. This translates into a bulk night time cooling rate of $\sim 0.15 \text{ K.hr}^{-1}$ for the first kilometer layer of air above the ground that forms the real 'thermal blanket'.

In order to gain a better understanding of the energy transfer, the downward LWIR flux at the surface was calculated using a radiative transfer model with 100 m vertical resolution from 0 to 10 km. The lapse rate was defined by setting the surface air temperature and relative humidity in the first 100 m layer. The lapse rate up to the saturation altitude was assumed to be -6.5 K.km^{-1} . Above this level, the saturated lapse rate was used. These lapse rate curves are illustrated in Figure 7. The changes in concentration (number density) for H_2O and CO_2 are also shown. The absorption and emission of H_2O and CO_2 were calculated at a minimum resolution of 0.01 cm^{-1} in intervals of 50 cm^{-1} from 200 to 2000 cm^{-1} . The spectral resolution was increased to accommodate the line density in the region of the main CO_2 band from 600 to 750 cm^{-1} . The calculations were performed using Excel worksheets containing the HITRAN spectral data for the individual H_2O and CO_2 lines.^[9] To facilitate the calculations, only the data for the principal isotopologues $^1\text{H}_2^{16}\text{O}$ and $^{12}\text{C}^{16}\text{O}_2$ were used and only lines with linestrengths above $10^{-23} \text{ cm}^{-1}/\text{molecule.cm}^{-2}$ were selected. These are plotted in Figure 8. This slightly underestimated the overall emission and absorption, but did not significantly alter the calculated flux differences for changes in absorption and emission due to changes in temperature and concentration. To avoid unnecessary effort, the spectra of other minor greenhouse gases such as methane, ozone and various halogenated hydrocarbons were not included in the radiative transfer calculations. Further details are given in Reference 7.

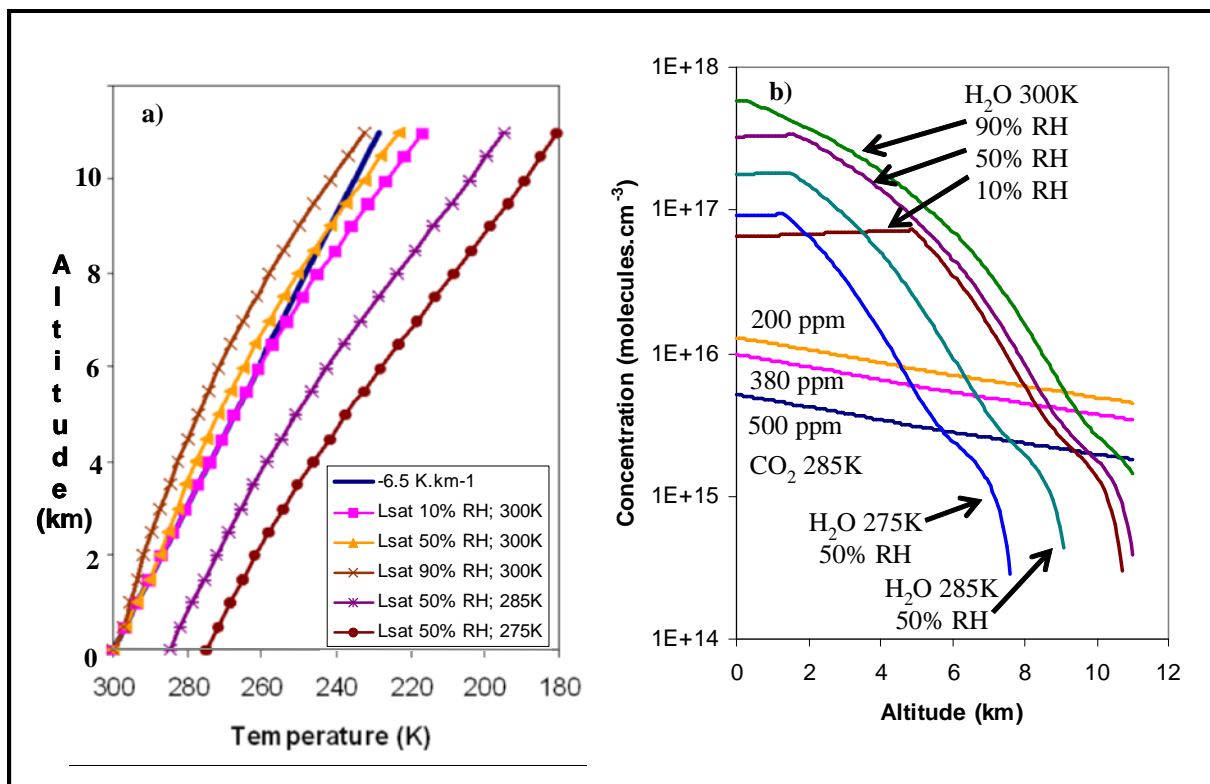


Figure 7: Calculated lapse rates and molecular concentrations vs. altitude. A lapse -6.5 K.km^{-1} was used up to the saturation point.

Figure 9 shows the downward atmospheric LWIR flux from H₂O and CO₂ for a surface temperature of 297 K and a starting air temperature of 295 K at the RH values shown. The CO₂ concentration was 380 ppm. The spectral resolution was 0.01 cm^{-1} and summary flux data are shown for spectral intervals of 50 cm^{-1} . To accommodate the large number of CO₂ lines between 600 and 750 cm^{-1} the spectral intervals were set to be 600, 620, 640, 660, 665, 670, 680, 700, 725 and 750 cm^{-1} with resolutions of 0.004, 0.001, 0.002, and 0.005 cm^{-1} . To compare the flux on the same spectral scale, the data were adjusted to a match the spectral interval of 50 cm^{-1} . The temperature difference of 2 K between the air and surface temperatures is representative of long term average ocean conditions, (see Figure 2a, b). The principal change in the LWIR flux spectral distribution is the decrease in downward flux in the 400 to 600 cm^{-1} spectral region with the decrease in RH. There is also a less pronounced decrease in flux with RH in the ‘edges’ of the LWIR window region from ~ 800 to 1300 cm^{-1} and a decrease in flux in the 1800 to 2000 cm^{-1} region.

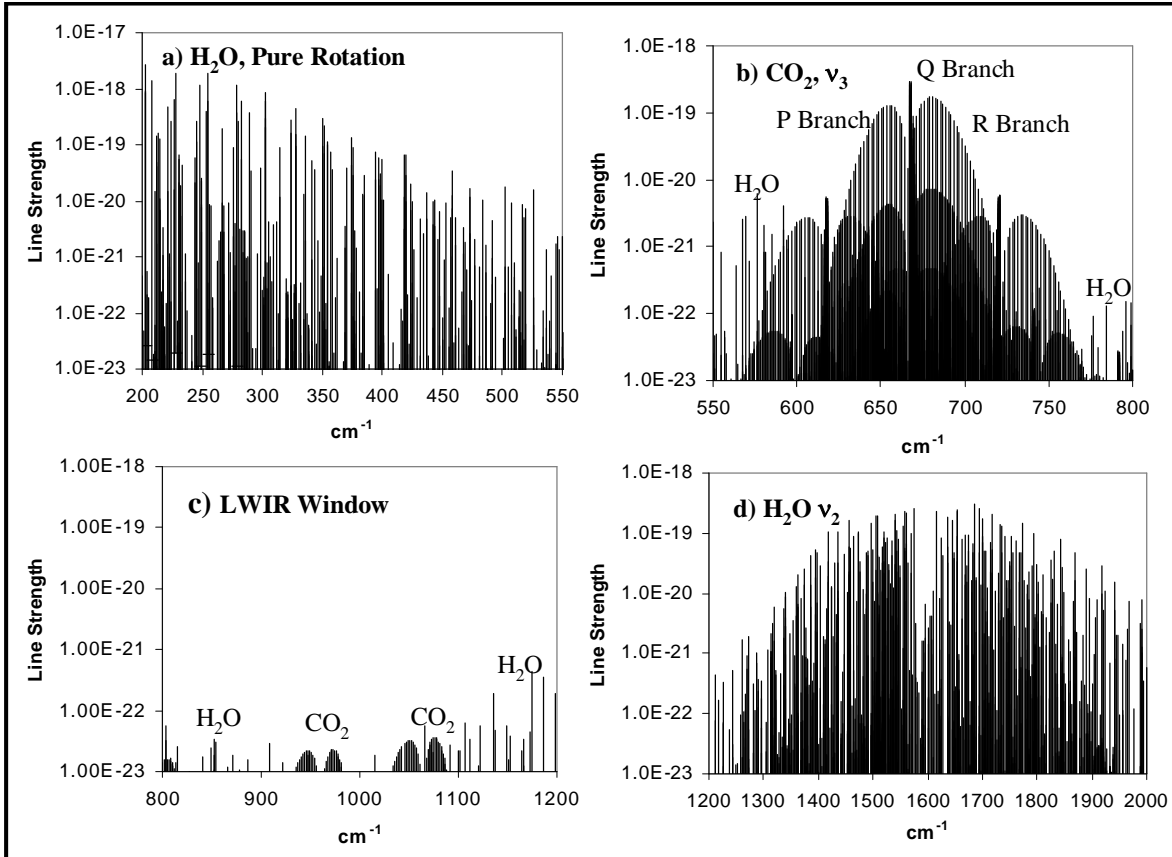


Figure 8: Truncated data set of linestrengths of $^1\text{H}_2^{16}\text{O}$ and $^{12}\text{C}^{16}\text{O}_2$ used in the radiative transfer calculations. ^[7,9]

The effect on the downward LWIR flux of changes in air temperature at a fixed RH of 50% for air/surface temperature combinations of 295/297, 285/287 and 275/277 K are shown in Figure 10. The trend in the change in flux with temperature is similar to that of the change with RH at a fixed temperature shown in Figure 9. The downward flux decreases with temperature. The RH defines the humidity relative to the saturated vapor pressure at the specified air temperature. The vapor pressure of water decreases significantly with temperature so that 50% RH at 275 K means that there is much less water in the air than 50% RH at 295 K. The vapor pressure curve of water with temperature is shown in Figure 11. ^[20] At 295 K the vapor pressure is 19.8 Torr and this decreases by almost a factor of 2 to 10.5 Torr at 285 K and by another factor of ~ 2 to 5.3 Torr at 275 K.

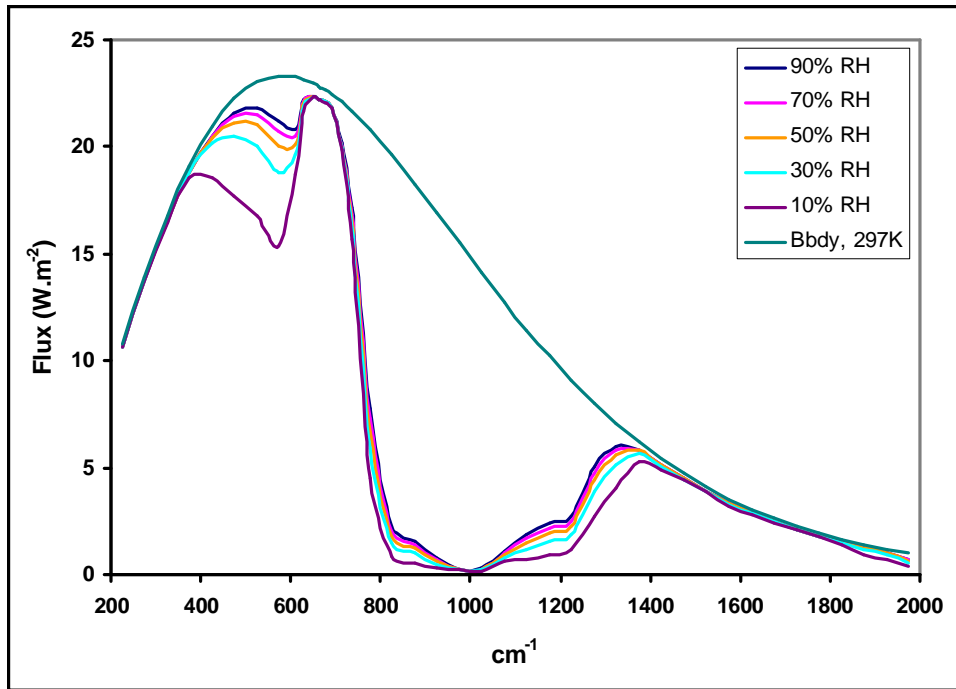


Figure 9: Downward LWIR flux at the surface for an air temperature of 295 K and a surface temperature of 297 K at the RH values shown. (H₂O and CO₂ only - truncated data set).

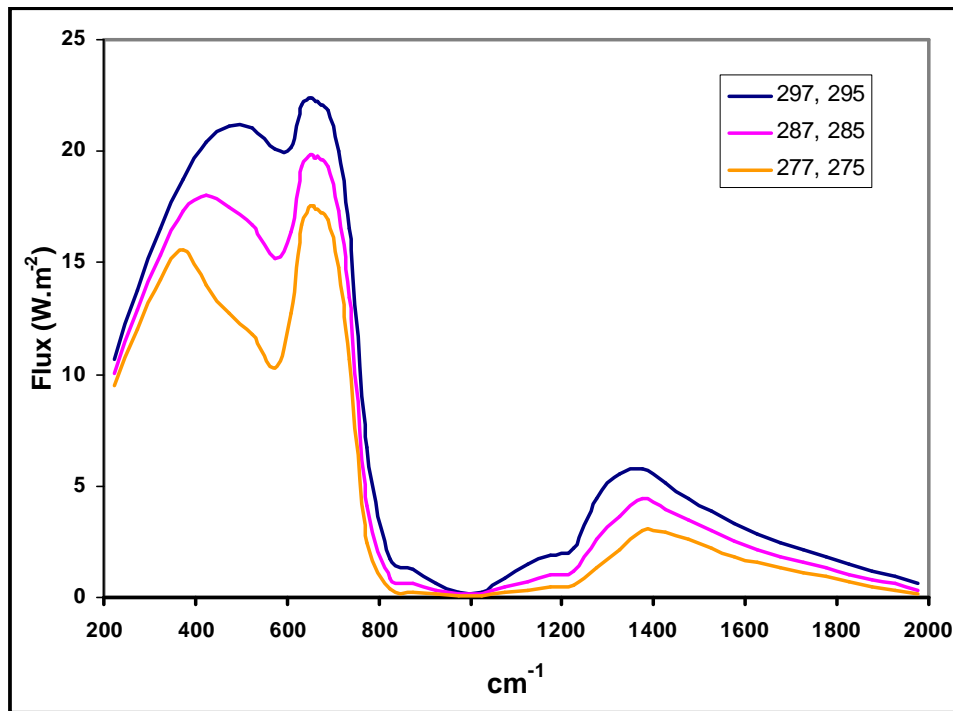


Figure 10: Downward LWIR flux at the surface for the surface/air temperature combinations shown at 50% RH. (H₂O and CO₂ only - truncated data set).

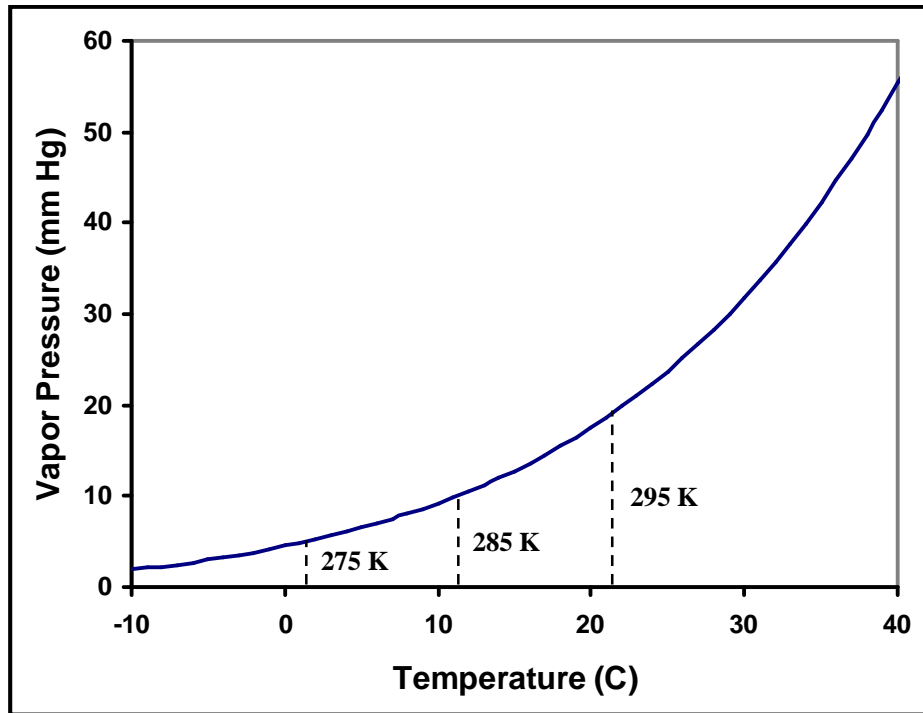


Figure 11: The vapor pressure of water from -10 to 40 C.

The variations in total downward LWIR flux for the cases calculated in Figure 9 and Figure 10 are summarized in Figure 12. In addition, data for the 325/295 K surface/air temperature cases at 10, 45, 50 and 90% RH are also included. These are very similar to the 297/295 K cases, since the downward flux is determined principally by the air temperature and humidity. It should be noted that Figure 12 only includes the contributions of $^1\text{H}_2^{16}\text{O}$ and $^{12}\text{C}^{16}\text{O}_2$ to the downward LWIR atmospheric flux. The contributions from other isotopologues of H_2O and CO_2 and other IR active gases such as CH_4 and O_3 are not included. Figure 13 shows the changes in flux relative to the 297/295 K, 50% RH case, to give the actual magnitude of the calculated flux changes. The flux increases by $\sim 36 \text{ W.m}^{-2}$ as the RH is increased from 10 to 90% RH at an air surface temperature of 295 K. The flux decreases by 94 W.m^{-2} as the air temperature is decreased from 295 to 275 K. The corresponding change in flux for a blackbody surface is 105 W.m^{-2} .

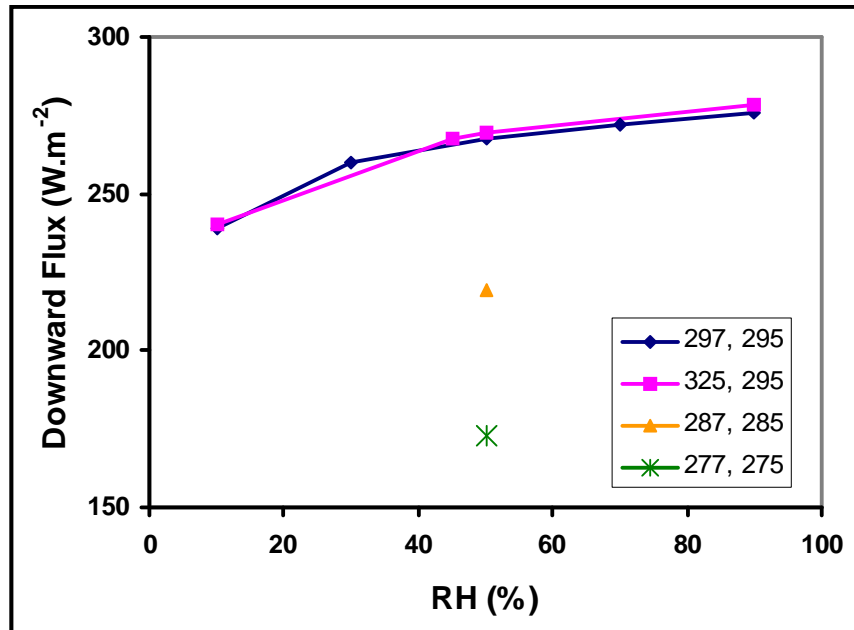


Figure 12: Variations in total downward LWIR flux calculated from the data presented in Figure 9 and Figure 10 above. The 325/295 case at 90, 70, 50, 30 and 10% RH is also shown.

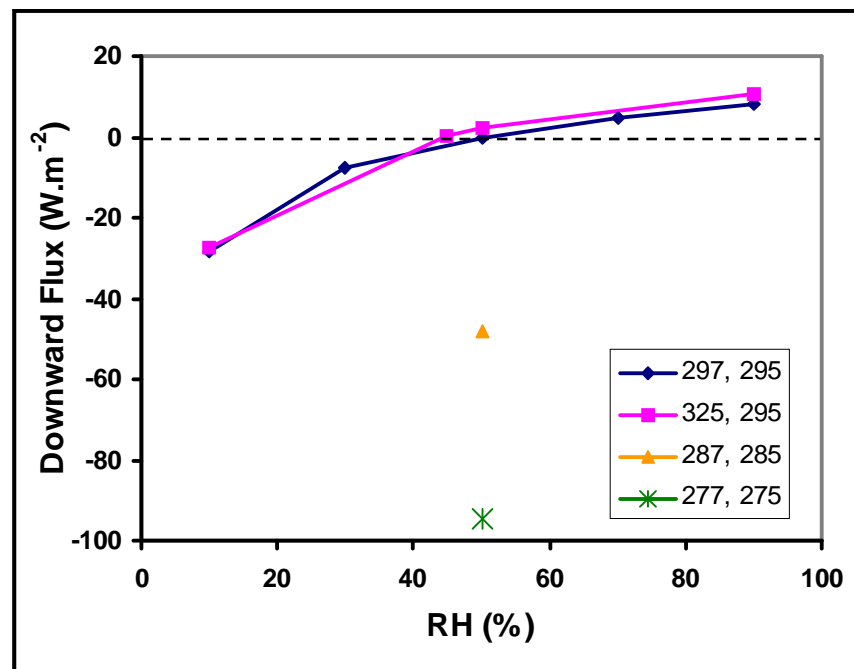


Figure 13: Flux changes shown in Figure 12 with the 297/295, 50% RH case flux subtracted.

The downward atmospheric LWIR flux reaching the surface originates mainly in the first kilometer layer above the surface. The spectrally resolved fluxes from altitudes above 1 km derived from the data used in Figure 9 are shown in Figure 14. The fraction of the total flux from altitudes > 1 km increases from approximately 7 to 14% as the RH decreases from 90 to

10%. The principal change occurs in the 400 to 600 cm^{-1} region, which is part of the H_2O rotational spectrum.

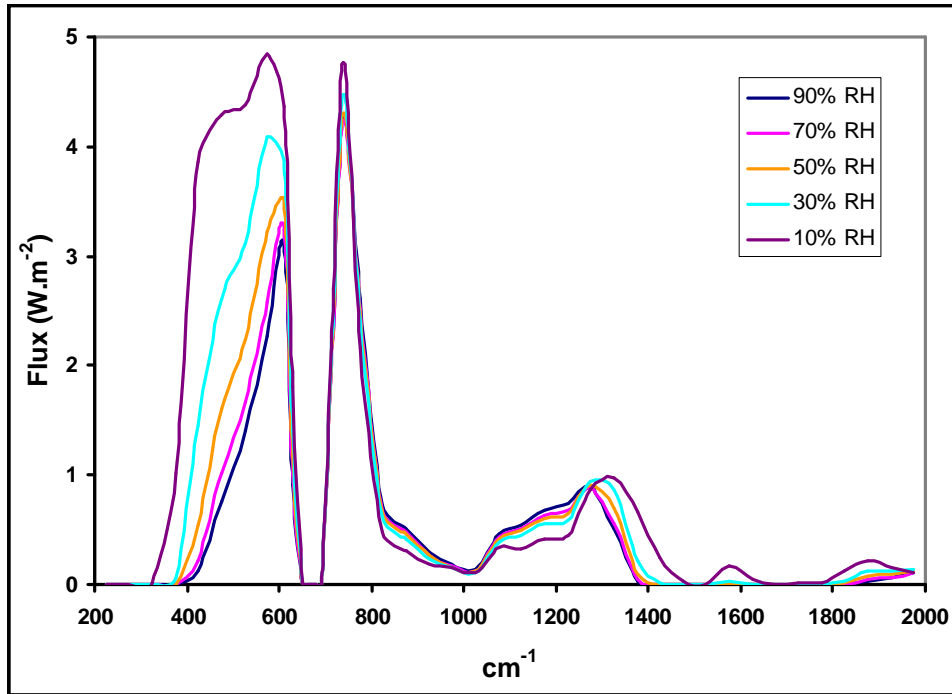


Figure 14: Downward LWIR flux originating above 1 km for the surface fluxes shown in Figure 9.

Figure 15 shows the total cumulative flux vs. altitude reaching the surface for the cases selected and Figure 16 shows the corresponding normalized fluxes. Usually, at least 90% of the total downward flux originates within the first kilometer layer above the surface.

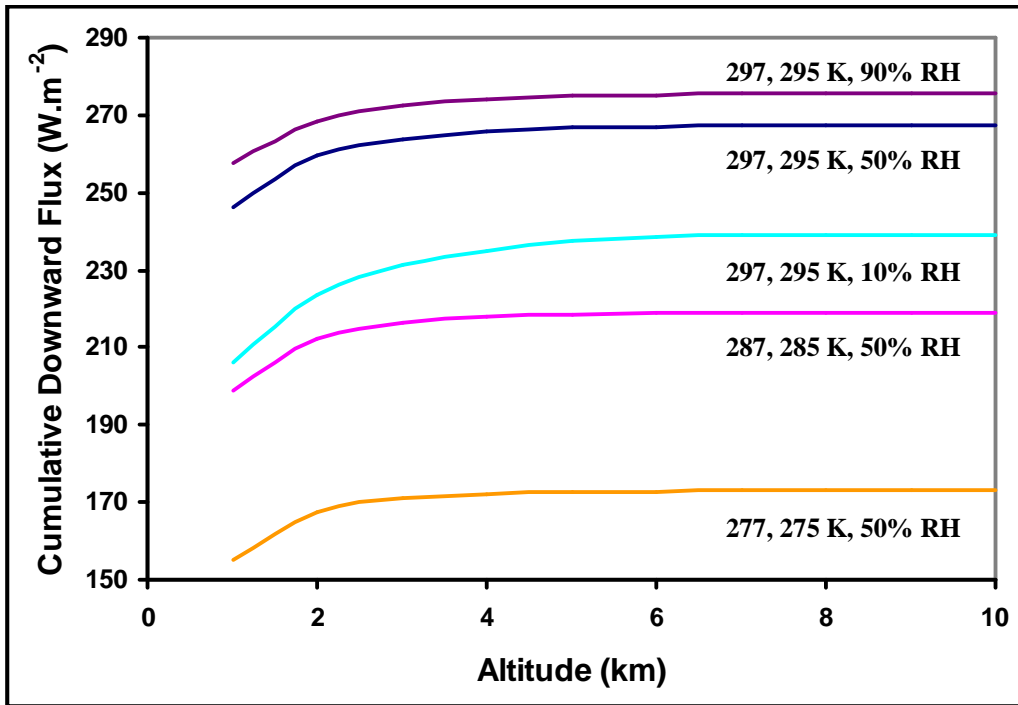


Figure 15: Cumulative downward flux vs. altitude for the cases shown.

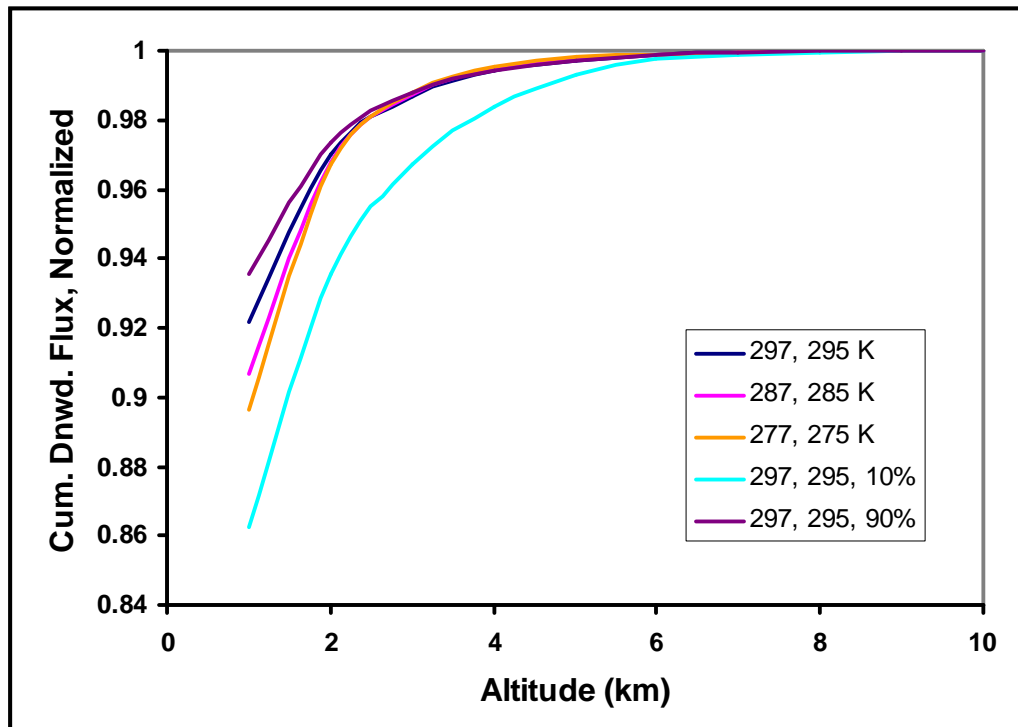


Figure 16: Normalized fluxes from Figure 15.

4.1: The Effect of Clouds on the Downward Atmospheric LWIR Emission

As moist air rises through the atmosphere it cools. When the water vapor pressure reaches saturation, condensation starts and clouds form. This usually occurs at altitudes above 1 km. The water or ice particles in the cloud act as blackbody radiators. The downward LWIR radiation from the cloud layer will partially close the LWIR atmospheric window, depending on the temperature of the cloud base. This is illustrated in Figure 17. The normalized downward atmospheric LWIR flux for a surface air temperature of 300 K is shown with black body emission curves for 292 and 277 K normalized to the 300 K blackbody flux. The 292 and 277 K temperatures represent cloud base heights of approximately 2 and 4 km based on the 300 K, 50% RH lapse rate. At 292 K, the downward LWIR flux from the cloud reduces the surface cooling flux through the window by ~80% and at 277 K this reduction is 65%.

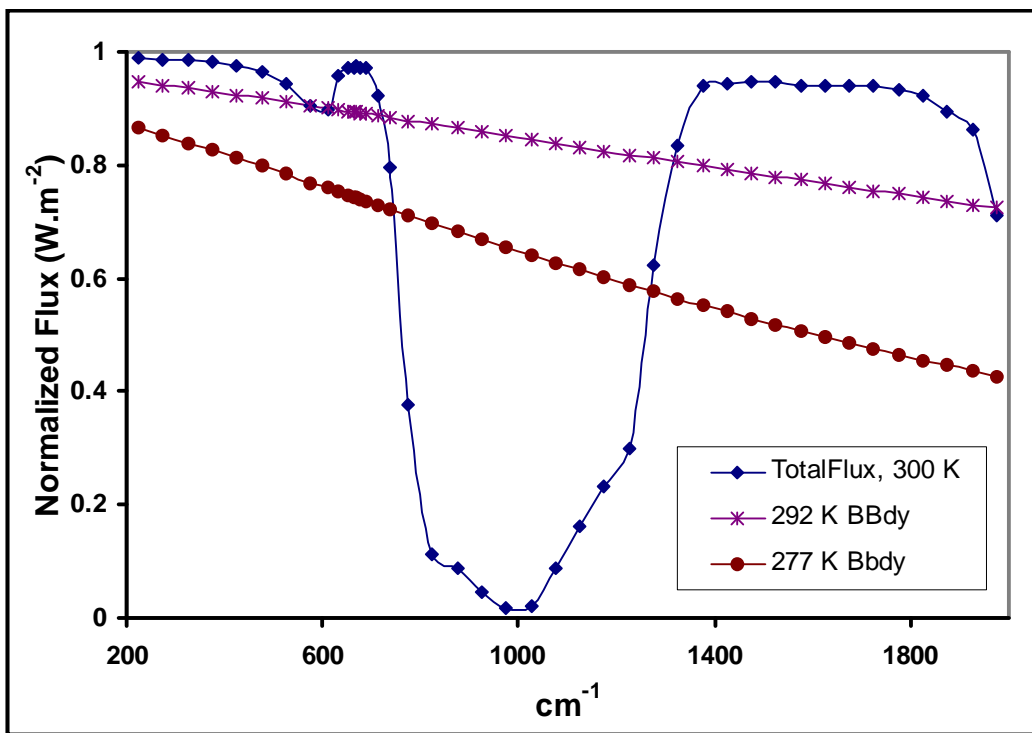


Figure 17: The effect of clouds on the LWIR window. (H_2O and CO_2 only - truncated data set).

5.0 Convective and Radiative Energy Transfer within the Atmosphere

The previous 3 sections have considered the surface energy transfer at the air-ocean and air-land interfaces and the downward LWIR flux reaching the surface from the atmosphere. Now we need to understand how the surface energy is transferred within the atmosphere. These energy transfer processes involve the convective mixing of moist air as it ascends through the atmosphere, the thermodynamics of the lapse rate, water condensation and the absorption and emission of LWIR radiation. The troposphere is an open thermodynamic system so that neither the volume nor the pressure remain constant as an air mass rises through the atmosphere. Without getting into the details of the thermodynamics of the ascent, the heat capacity of 1 m^3 of

air in the lower troposphere is approximately 1 kJ. An increase in altitude of 150 m at a lapse rate of $-6.5\text{K}\cdot\text{km}^{-1}$ will produce a decrease in temperature of 1 K which means that the air has performed 1 kJ of work in expansion against the air pressure to ascend 150 m. The pressure difference in turn is set by the weight of the air and the downward force of gravity. Thermal energy is lost by LWIR radiation to space at the top of the atmosphere and this energy is replaced by the conversion to thermal energy of the solar energy reaching the surface. The bulk of this solar thermal energy is transported through the atmosphere by convection. This is a mass transport process, not a radiative one. The so called ‘greenhouse effect cooling’ is really just the heat that is converted to mechanical work to overcome the force gravity as the air ascends through the atmosphere. There is also some direct heating of the troposphere by the IR and NIR components of the solar flux through molecular absorption. The upper atmosphere is also heated by the direct absorption of the solar UV flux. The thermal energy produced at the surface consists of four components. Direct heating of the air at the surface produces convection. Some of the excess LWIR radiation produced because the surface is warmer than the adjacent air is absorbed by the atmosphere near the surface, mainly within the first 100 m and is added to the air convection. The remainder of the LWIR flux is emitted directly to space through the LWIR atmospheric window. Over land, depending on the surface water content, some of the solar flux is converted into a latent heat flux through the evaporation of water. This cools the surface by evaporation and releases the latent heat into the troposphere by condensation and cloud formation, usually at altitudes above 1 km. The latent heat flux is often the dominant surface cooling flux over the oceans. The energy transfer processes are illustrated above in Figure 1 and the diurnal energy transfer cycle over land for full summer sun conditions is shown in Figure 6.

As the moist air from the surface ascends through the atmosphere, it establishes a local lapse rate. This is often calculated using the simplified assumptions that the air remains saturated during the ascent and that there is no mixing with the surrounding air. However, regardless of the details, the temperature and pressure decrease significantly with altitude. Typical values near the tropopause at a nominal 11 km altitude are 220 K and 0.25 atm.^[21] The water vapor concentration (number density in molecules. cm^{-3}) decreases by about three orders of magnitude and the CO_2 concentration decreases by a factor of ~ 5 . This is illustrated above in Figure 7.

The LWIR absorption and emission of the individual molecular lines in the atmosphere depends on the number density, the temperature and the pressure. The number density determines the number of absorbing molecules, the temperature determines the Maxwell Boltzmann population distribution of the molecular energy levels and the pressure determines the linewidth through collisional broadening. This follows from the Heisenberg uncertainty principle between time and energy.^[22] In the troposphere the excited rotation-vibration state lifetime is significantly reduced by molecular collisions. This time-energy uncertainty increases the linewidth. The total absorption and emission also depends on the line spacing or the overlap of the individual line profiles.

The upward and downward LWIR fluxes in the troposphere are not equivalent because of the linewidth effects. The upward LWIR flux has to be divided into two fractions, a free photon flux that is not reabsorbed and a photon exchange fraction that is reabsorbed by the IR active molecules in the atmosphere. The free photon flux increases with altitude. There is no

downward free photon flux that originates in the troposphere, because the molecular linewidth and the pressure and temperature increase as the altitude decreases. This is illustrated in Figure 18.

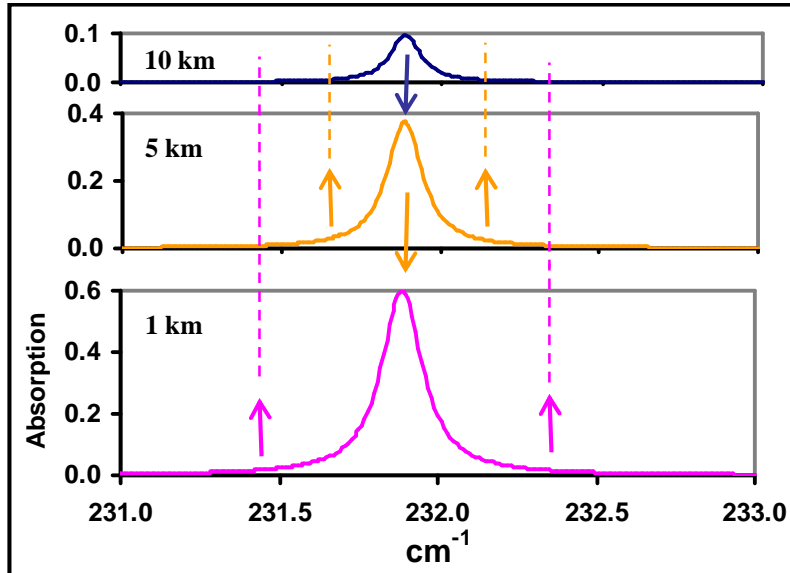


Figure 18: Change in linewidth with altitude. Photons emitted from the wings of the pressure broadened lines in the lower troposphere are not reabsorbed at higher altitudes.

In general, an air parcel in the troposphere emits equal amounts of LWIR flux in the upward and downward directions. The air parcel will also absorb LWIR radiation from the air layers above and below. Usually the downward emitted flux and the upward absorbed flux are similar, whereas the absorbed downward flux from the cooler air layers above will be less than the upward emitted flux. The net effect is therefore a cooling of the atmosphere. This is illustrated in Figure 19. For an air layer 100 m thick, the net cooling in the middle troposphere is approximately $2 \text{ W}\cdot\text{m}^{-2}$. If the heat capacity of this air volume is 85 kJ, it will take the air parcel ~ 12 hours to cool by 1 K. The heat lost through LWIR emission is replaced by convective mixing with warmer air from below. The energy transfer from convection can occur at a much faster rate than by radiative transfer, so the tropospheric temperature profile is maintained by convection, not by radiative transfer. The local lapse rate is re-established each day by the convective ‘impulse’ of the solar thermal energy from the surface.

Since the atmosphere absorbs most of the excess LWIR flux from the surface within the first kilometer, this absorption process will now be examined in more detail.

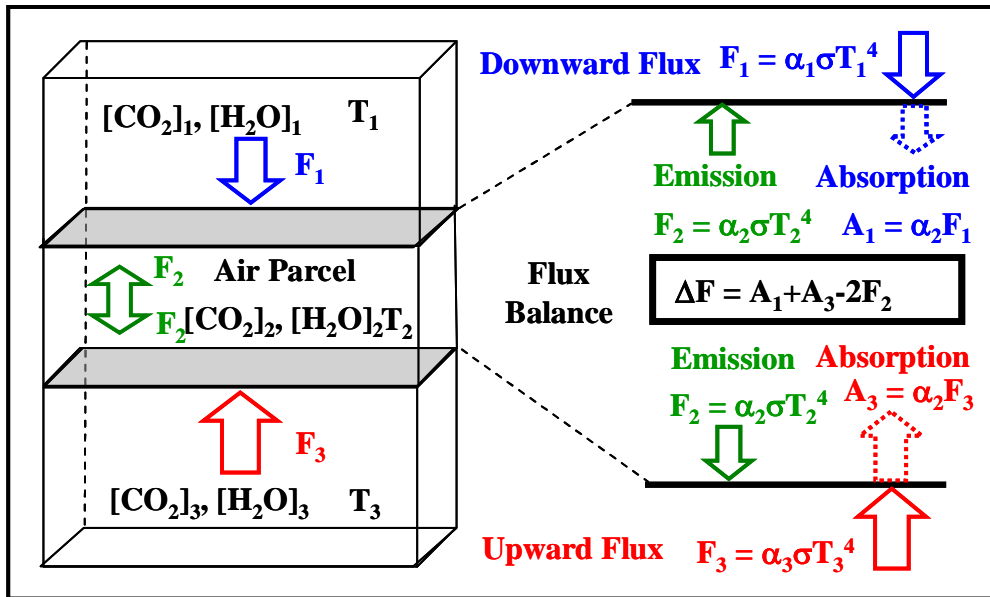


Figure 19: The radiative flux balance in the troposphere. The IR active gases in the air parcel emit flux F_2 in both directions. They also absorb part of the downward flux F_1 and the upward flux, F_3 from the surrounding air. The net balance of these terms determines the heating or cooling produced by the greenhouse effect. In general, the net balance leads to cooling, unless the air parcel is close to a warmer ground surface.

5.1 The Absorption of LWIR Radiation near the Surface

When the surface is warmer than the air above it, there is a net absorption and heating of the atmosphere by the LWIR radiation. The upper limit to the absorption is simply the difference in the blackbody emission between the surface temperature and the ‘effective’ temperature of the air near the surface. This of course follows from the Second Law of Thermodynamics and the Kirchoff Exchange Law. The only temperature record that we have is the MSAT record, so this by default is the baseline effective air temperature. Almost all of the excess LWIR radiation from the surface is absorbed within the first kilometer above the surface and most of this is absorbed in the first 100 m. Figure 20 shows the spectrally resolved net absorption through the atmosphere up to 6 km for a surface temperature of 325 K, a surface temperature of 295 K, an RH of 50% and a CO₂ concentration of 380 ppm. As discussed above, the model spectral resolution changes in the region of the CO₂ band because of the increase in the line density. The data in the Excel 3-D plots are displayed as series with equal increments, not as a scaled x-y plot. The scale change is indicated on the figure. Figure 21 shows the calculated absorption of Figure 20 plotted on an enlarged scale to show the cooling effects above 1 km in more detail. The mysterious bulk ‘forcing’ and ‘feedback’ effects required by the concepts of ‘equilibrium radiative forcing’ have no basis in the physical reality of the detailed spectrally resolved energy transfer.

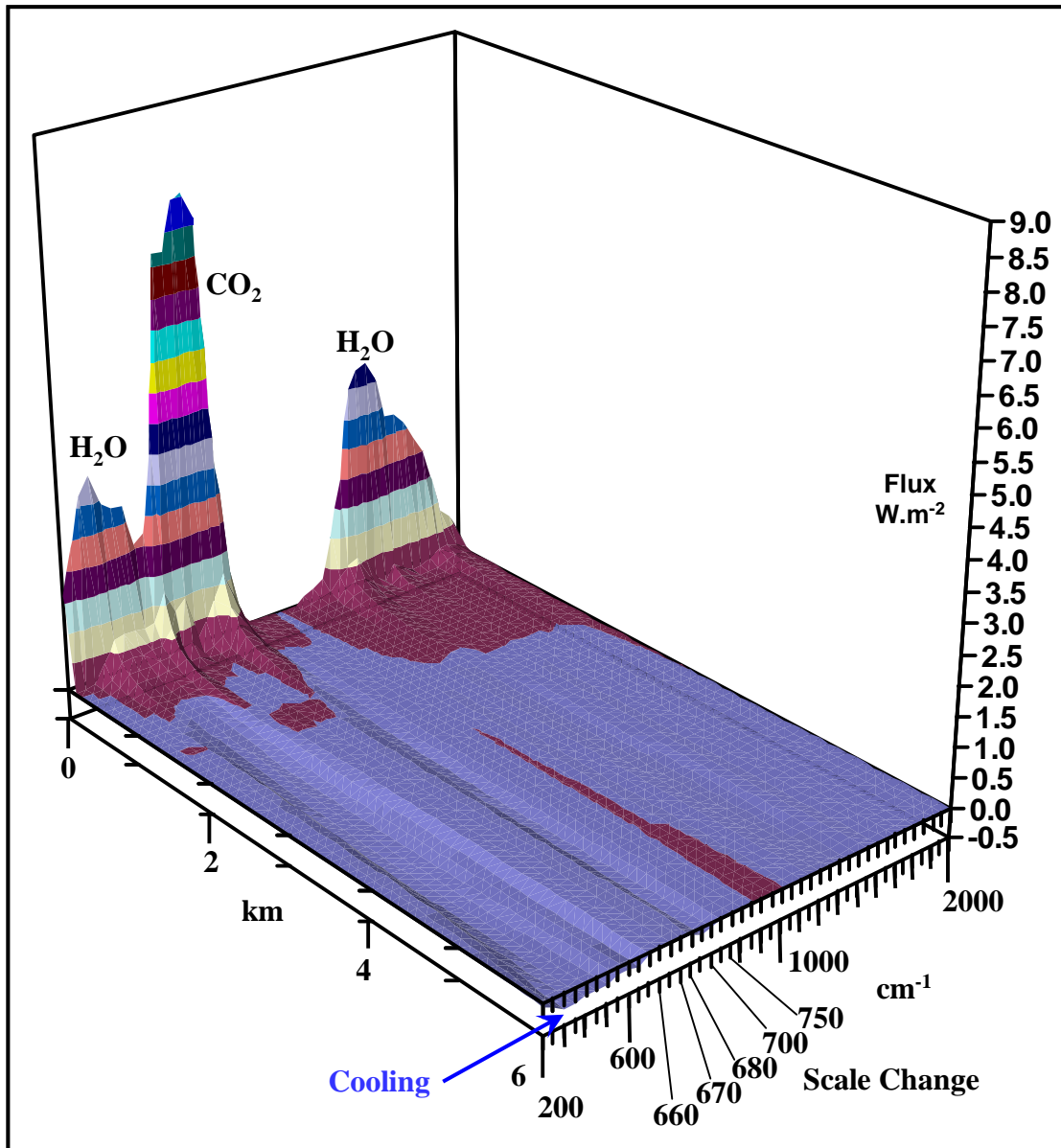


Figure 20: Spectrally resolved absorbed flux vs. altitude. Only the H₂O and CO₂ bands are shown. The surface temperature is 325 K, the surface air temperature is 295 K, and the RH is 50%. Most of the LWIR radiation from the ground is absorbed in the first 100 m. (H₂O and CO₂ only - truncated data set).

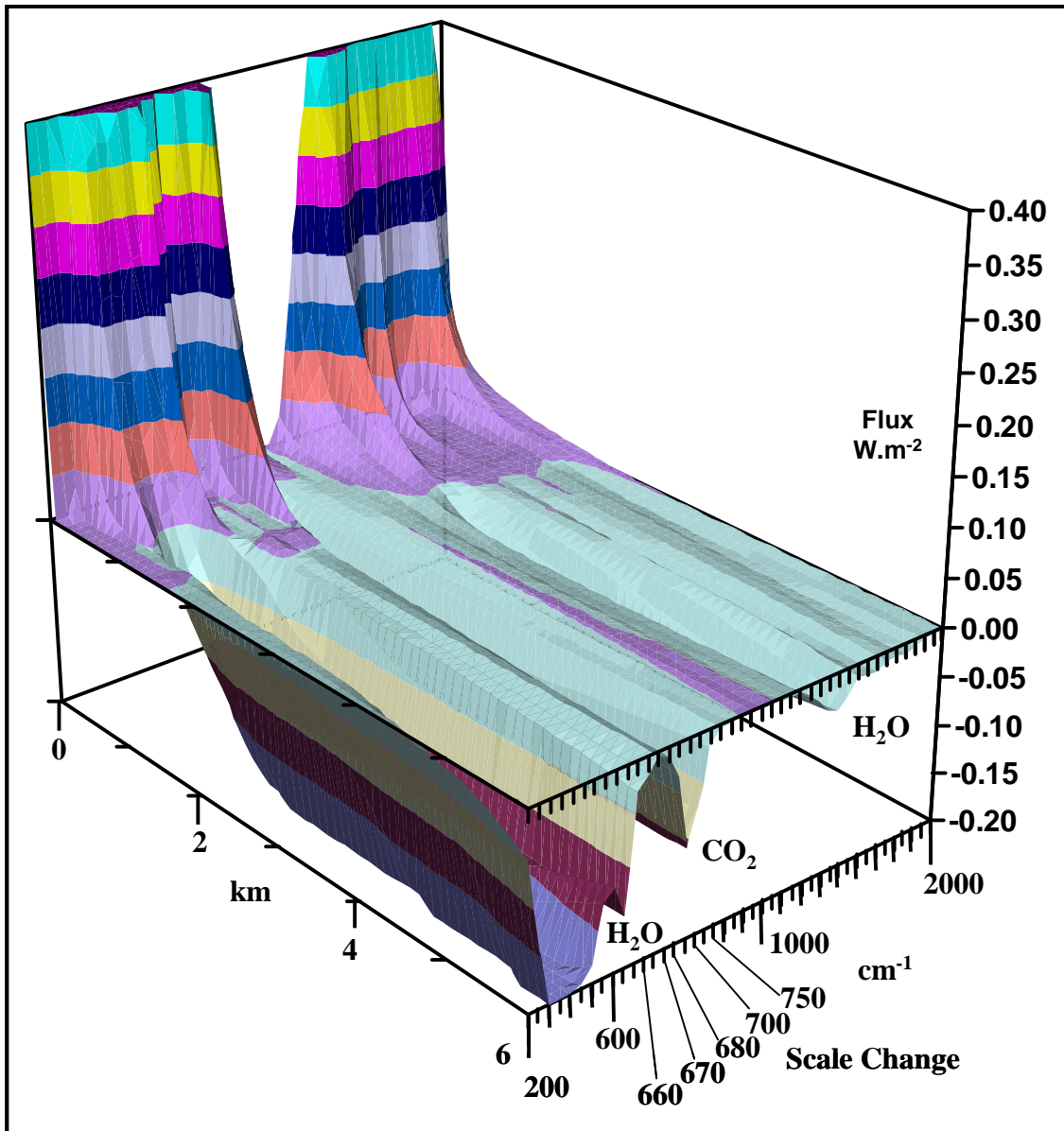


Figure 21: Data from Figure 20 plotted on an enlarged scale to show the cooling effects above 1 km.

In order to evaluate the heating effects near the surface, the radiative transfer model was modified to include path lengths near the surface of less than 100 m. The higher spatial resolution of the absorption near the surface is illustrated in Figure 22. The temperature and concentration conditions are the same as in Figure 20. The path lengths are from 0.5 m to 1 km. The upper limit to the absorption is simply the difference between the blackbody emissions at the surface and air temperatures of 325 and 295 K within each spectral band. The resolved absorption data were normalized using the spectrally resolved blackbody emission at 325 K. The normalized absorption data are plotted in Figure 23.

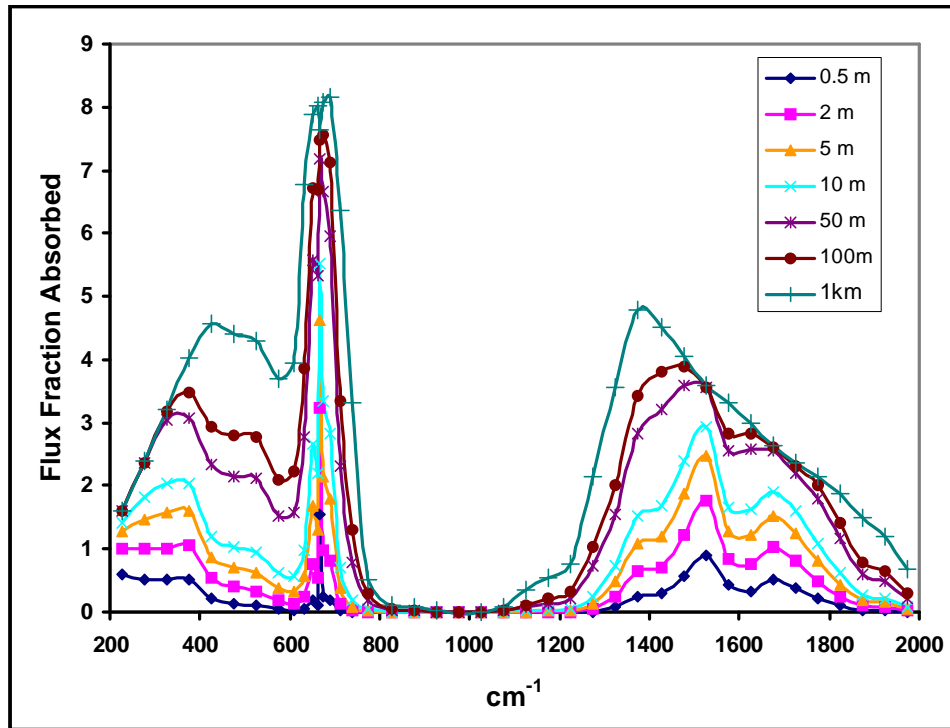


Figure 22: Spectrally resolved LWIR flux absorbed by air layers near the ground. Surface temperature is 325 K, air temperature is 295 K, CO₂ concentration is 380 ppm, RH is 50%. Path lengths are from 0.5 m to 1 km. (H₂O and CO₂ only - truncated data set).

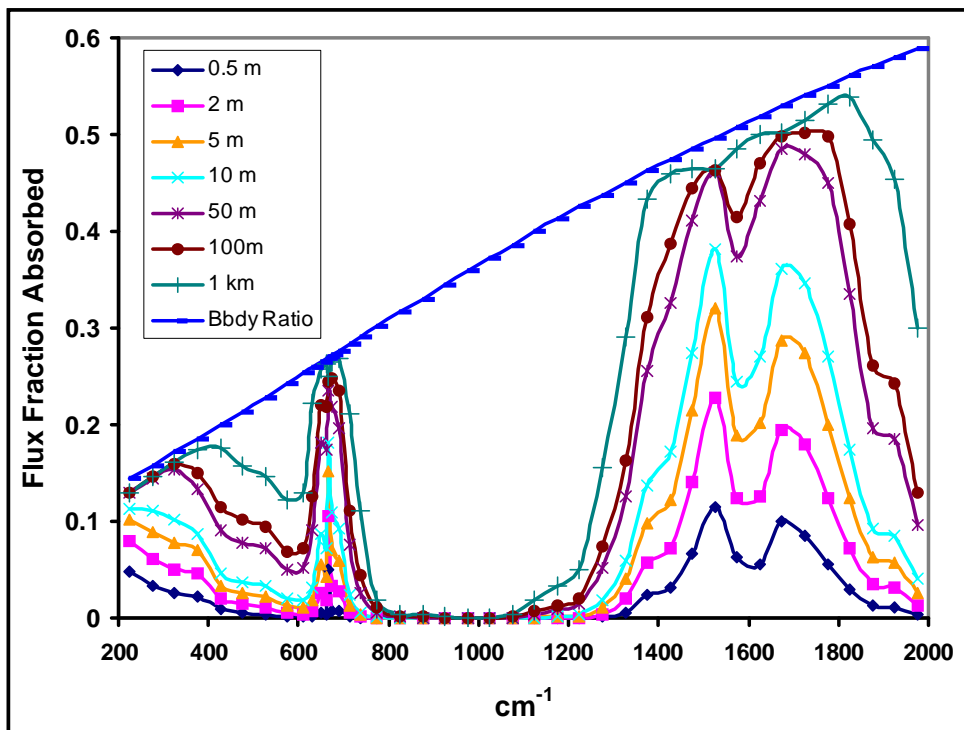


Figure 23: LWIR flux absorbed by air layers near the ground from Figure 22 normalized to the 325 K spectrally resolved blackbody emission. For reference, the 295 K blackbody limit is also shown.

Figure 24a shows the total, cumulative flux absorbed as a function of path length up to 1 km. The cumulative flux up to 10 m path length is shown on an expanded scale in Figure 24b. The approximate contributions of H₂O and CO₂ are also shown. The H₂O contribution was estimated by adding the flux from the spectral regions 200 to 550 cm⁻¹ and 1200 to 2000 cm⁻¹. The CO₂ contribution was estimated from the total flux in the spectral region from 550 to 800 cm⁻¹. This spectral region also includes some H₂O lines. At 1 km, H₂O absorbs ~75% of the total flux. This increases to 90% at 2 m and 96% at 0.5 m.

The effect of a 100 ppm increase in CO₂ from 280 to 380 ppm on the absorption at 2 m above the ground is shown in Figure 25a. The surface, air temperature combinations of 277, 275 K; 287, 285 K, 297, 295 K; 310, 295 K and 325, 295 K are shown at 50% RH. The maximum increase in absorption occurs for the 325, 295 K case. This is still only 0.25 W.m⁻² for a temperature difference of 30 K. Figure 25b shows the effect on the absorbed flux at 2 m of increasing the RH from 10 to 90%. For the 297, 295 K case, the increase in H₂O absorption is 0.8 W.m⁻² and for the 325, 295 K case, the increase is 12 W.m⁻². Clearly, an increase in absorption at 2 m above the ground caused by a 100 ppm increase in CO₂ concentration cannot be detected in the MSAT record. This is before the convective and latent heat terms are included.

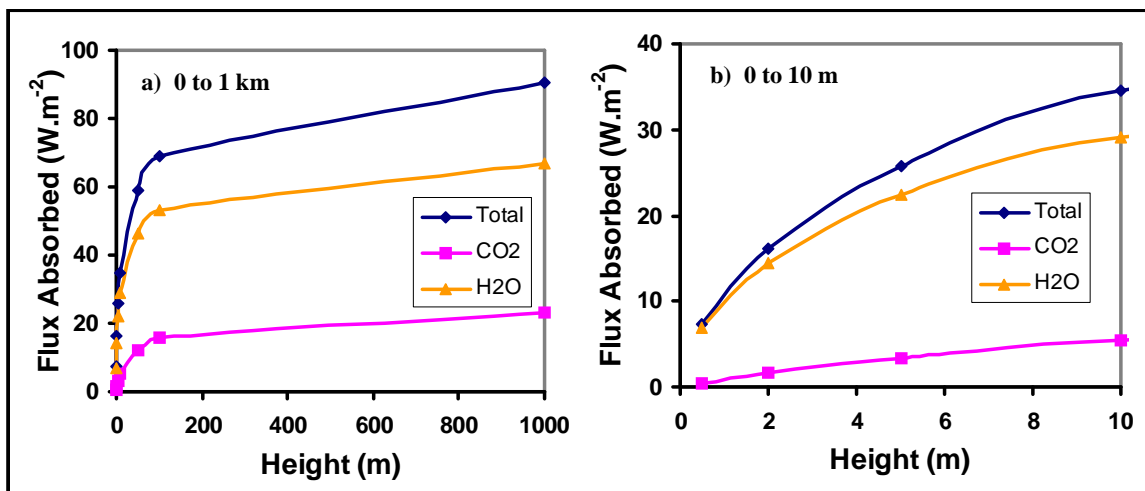


Figure 24: a) Total (cumulative) flux absorbed up to 1 km from the ground. The contributions to the absorption from H₂O and CO₂ are also shown separately. b) The absorption from 0.5 to 10 m on an enlarged scale. Data derived from Figure 22. At 1 km, H₂O absorbs 75% of the flux. This increases at shorter path lengths to 90% at 2 m and 96% at 0.5 m.

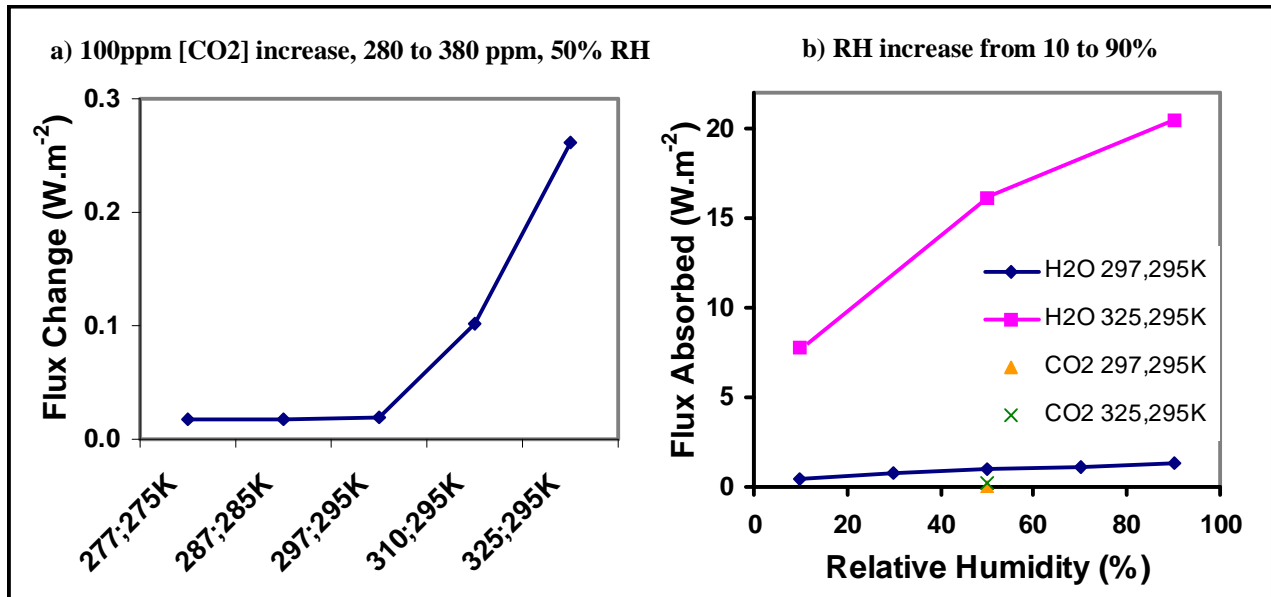


Figure 25: Effect of a 100 ppm increase in CO₂ concentration and changes in RH on the LWIR flux absorbed at 2m above the ground. (a) There is a slight increase in the absorbed flux at 2 m above the ground when the CO₂ concentration is increased from 280 to 380 ppm. For a 30 K surface-air temperature difference it is still only 0.25 W.m⁻². (b) The corresponding change in flux for a change in RH from 10 to 90 % is 12 W.m⁻². For a thermal gradient of 2 K the RH flux change is reduced to 0.8 W.m⁻².

6.0 The Upward Flux Leaving the Atmosphere

The clear sky upward flux leaving the atmosphere consists of two components, the flux emitted by the IR active molecules in the atmosphere and the direct LWIR flux from the surface. Figure 26 shows the calculated total upward LWIR flux and the surface and atmospheric components for the 297 K surface temperature, 295 K air temperature, 50% RH case. The emission is calculated for the truncated data set of H₂O and CO₂ lines only. Figure 27 shows the flux from Figure 26 normalized using the 297 K surface black body emission. The surface emission occurs mainly in the LWIR atmospheric transmission window between ~800 and 1200 cm⁻¹. [Note: the O₃ and CH₄ bands that are not shown will partially block the LWIR window]. There is also a partial ‘window’ in the 400 to 600 cm⁻¹ region, which is part of the H₂O rotation band. The upward flux is emitted from a range of altitudes in the atmosphere. As the temperature decreases with altitude, the H₂O emission shifts to lower energy from the ν₂ vibrational band to the pure rotation band. The line narrowing and the transition from Kirchoff exchange to free LWIR photon flux also occurs at lower altitudes for H₂O than for CO₂. This can be seen as a decrease in the upward emission in the 650 cm⁻¹ CO₂ ν₃ band. The CO₂ flux is emitted from a higher altitude than H₂O. The emission temperature is therefore lower.

If the surface temperature is increased in the radiative transfer model with the surface air temperature and the RH fixed, the upward surface emission will increase, but the atmospheric emission will remain almost the same. This is because the surface emission is absorbed in the lower troposphere and the upward emission is determined by the lapse rate in the upper troposphere. This is discussed in more detail in the next Section. The change in surface emission with surface temperature is illustrated in Figure 28.

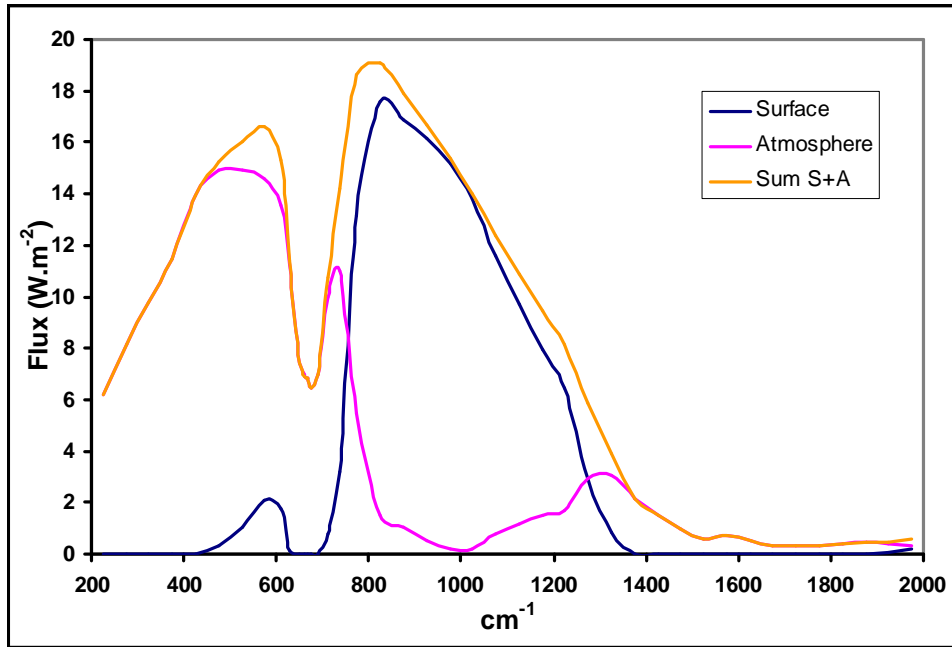


Figure 26: Upward flux leaving the atmosphere calculated for the limited H_2O and CO_2 line data set only. The surface emission, atmospheric emission and their sum are shown for the 297, 295 K, 50% RH case.

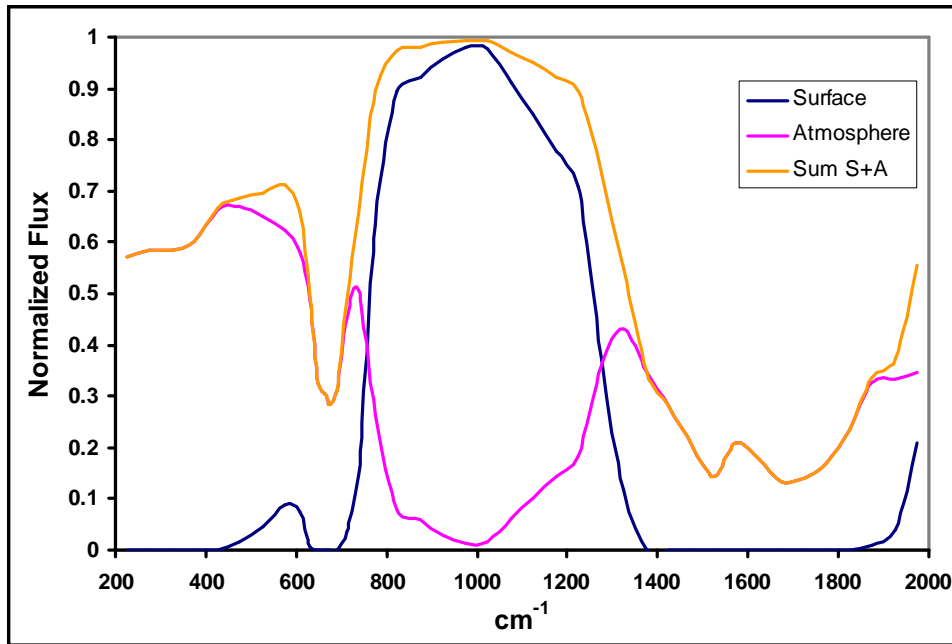


Figure 27: Flux from Figure 26 normalized to the 297 K blackbody emission.

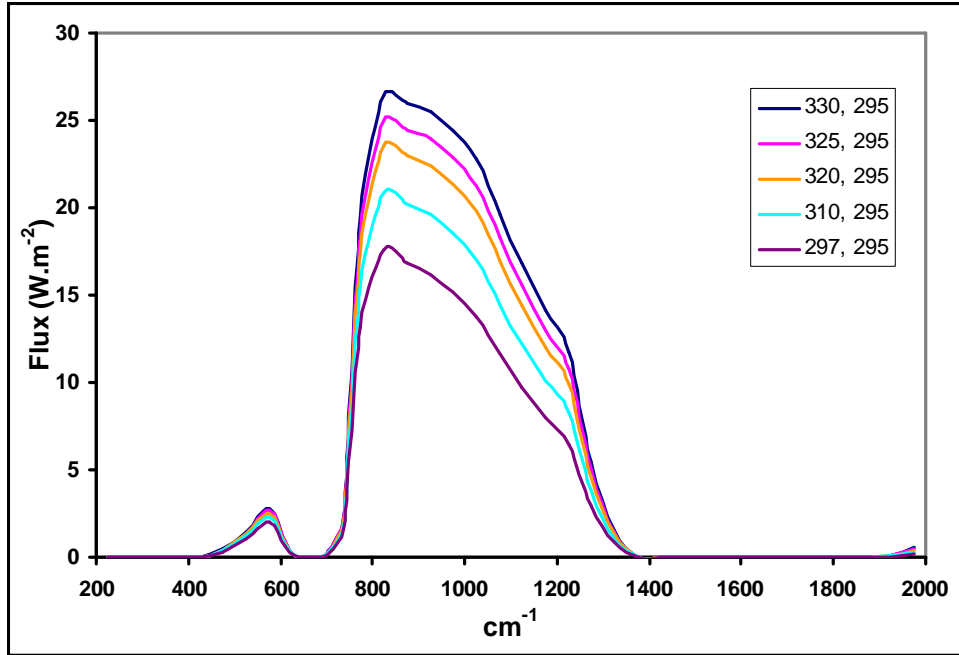


Figure 28: Variation in the upward surface flux as the surface temperature is changed for a fixed air surface temperature and RH, 295 K and 50% RH. The O₃ and CH₄ absorption bands are not shown.

The surface and atmospheric upward LWIR emission components and their sum for 3 different surface and air temperatures, 297, 295 K; 287, 285 K and 277, 275 K at an RH of 50% for each air temperature are shown in Figure 29. In the 200 to 600 cm⁻¹ region, the total upward flux remains almost constant. The decrease in atmospheric emission is balanced by an increase in the upward surface flux. The upward surface emission in the LWIR window region decreases with temperature as expected. The corresponding normalized fluxes are shown in Figure 30. The normalized flux can be interpreted as an indicator of the spectral emission temperature. The higher the value, the closer the emission is to the black body surface temperature.

The surface and atmospheric upward LWIR emission components and their sum for 3 different humidities, 90, 50 and 10 % RH at a surface, air temperature combination of 297, 295 K are shown in Figure 31. The change in total upward flux in the 200 to 600 cm⁻¹ region is again quite small because the decrease in upward atmospheric emission with decreasing humidity is compensated by an increase in the upward surface emission. A similar compensation occurs in the LWIR transmission window to keep the total upward flux almost the same over the 10 to 90 % humidity range. The corresponding normalized flux values, with each data set normalized to its own blackbody emission surface temperature are shown in Figure 32.

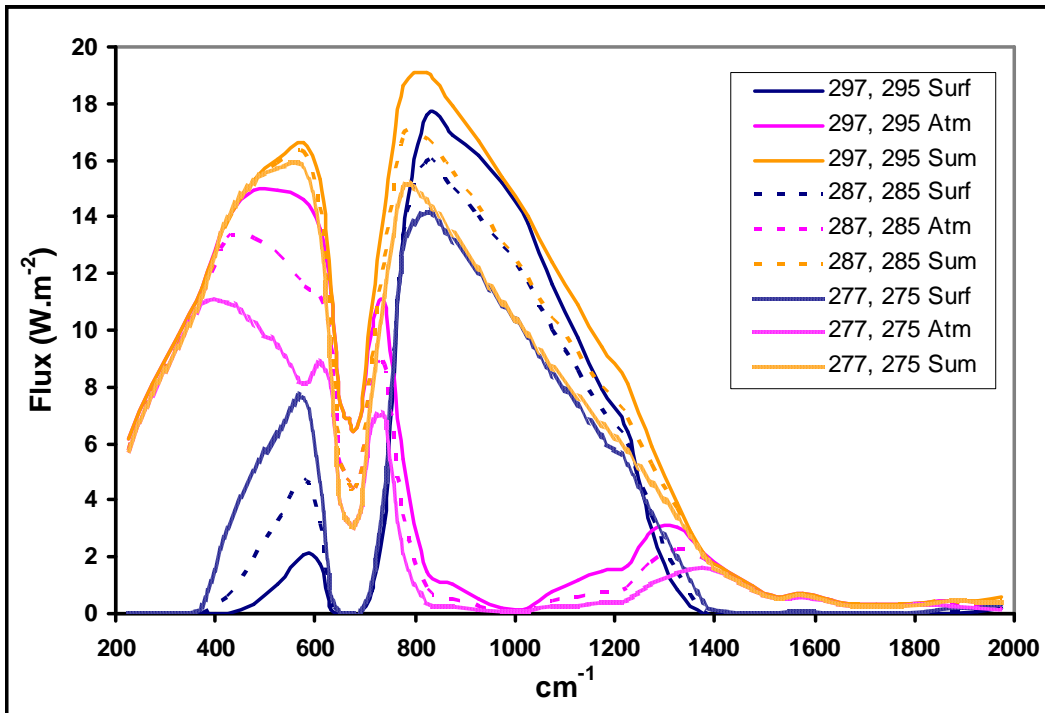


Figure 29: Upward emission for surface, air temperature combinations of 297, 295 K; 287, 285 K and 277, 275 K at 50% RH.

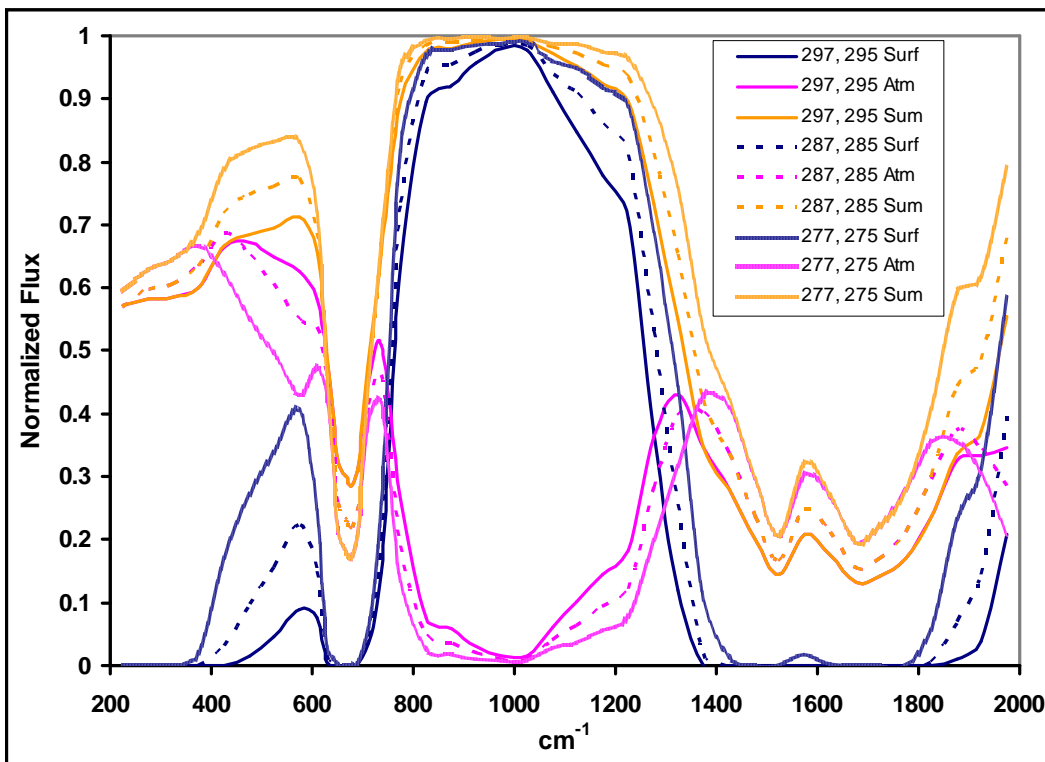


Figure 30: Normalized fluxes from Figure 29. Each set is normalized to the surface temperature emission used in the calculation.

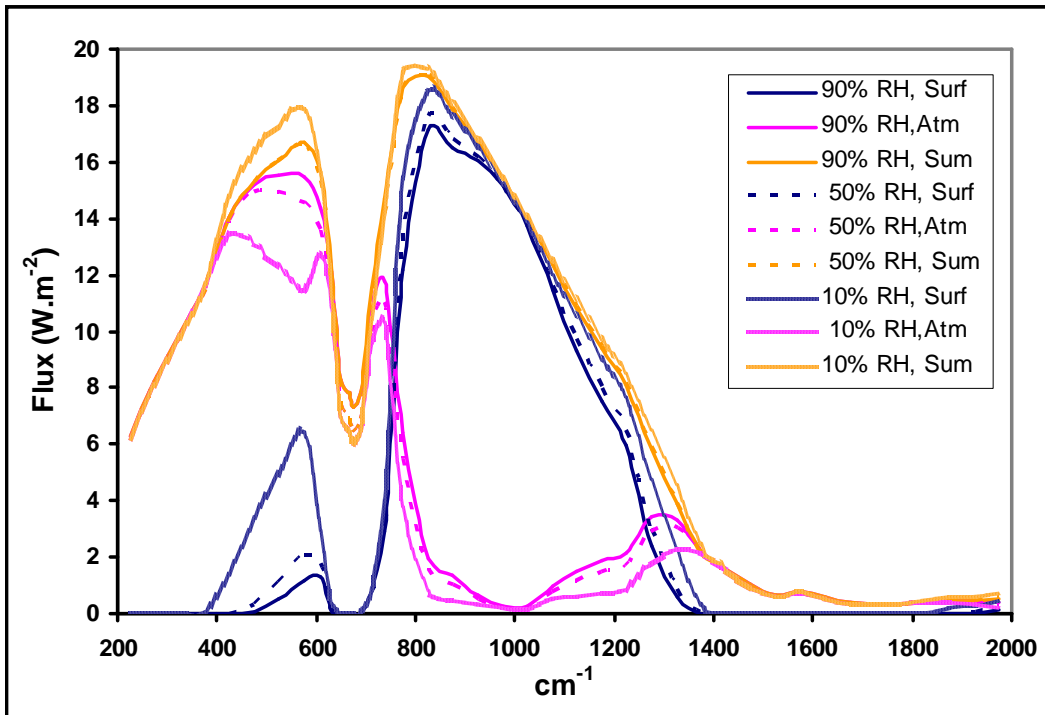


Figure 31: Upward emission for a surface, air temperature combination of 297, 295 K at 90, 50 and 10% RH.

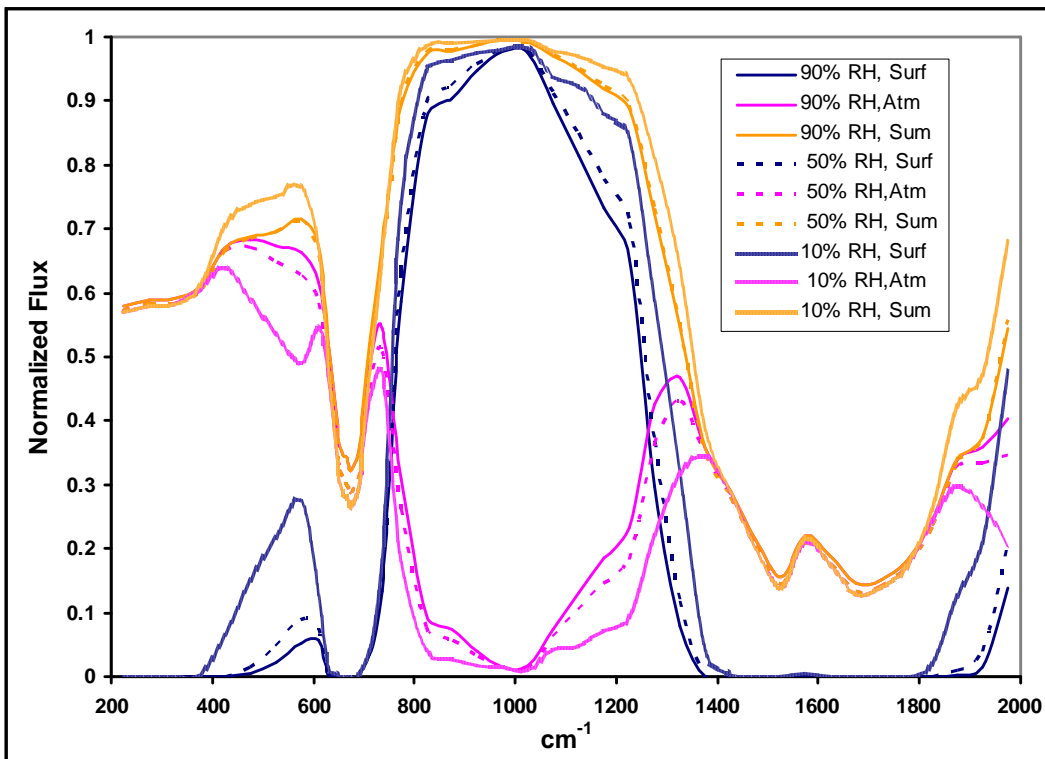


Figure 32: Normalized fluxes from Figure 31.

In Section 4.0, it was shown that most of the downward atmospheric LWIR flux reaching the surface, usually >90% originates within the first kilometer above the surface. Similarly, less than 10% of the total upward atmospheric LWIR flux leaving the atmosphere originates from within the first kilometer above the surface, except at low temperatures. Figure 33 shows the spectrally resolved total upward atmospheric flux and the flux originating from the first kilometer above the surface for the 297, 295 K; 287, 285 K and 277, 275 K cases shown in Figure 29. Figure 34 shows the ratio of the spectrally resolved 1 km flux to the total flux derived from the data used in Figure 33. Figure 35 and Figure 36 show the same data for the 297, 295 K, 10, 50 and 90% RH cases shown in Figure 31. Figure 37 summarizes the ratios (%) for the total fluxes derived from the data shown in Figure 29 and Figure 31. Less than 10% of the total flux comes from the first km layer except for the 277, 275 K case. The ratio for parts of the spectrally resolved flux, particularly in the LWIR window region may be higher than 10%, but the total flux ratio is still less than 10%.

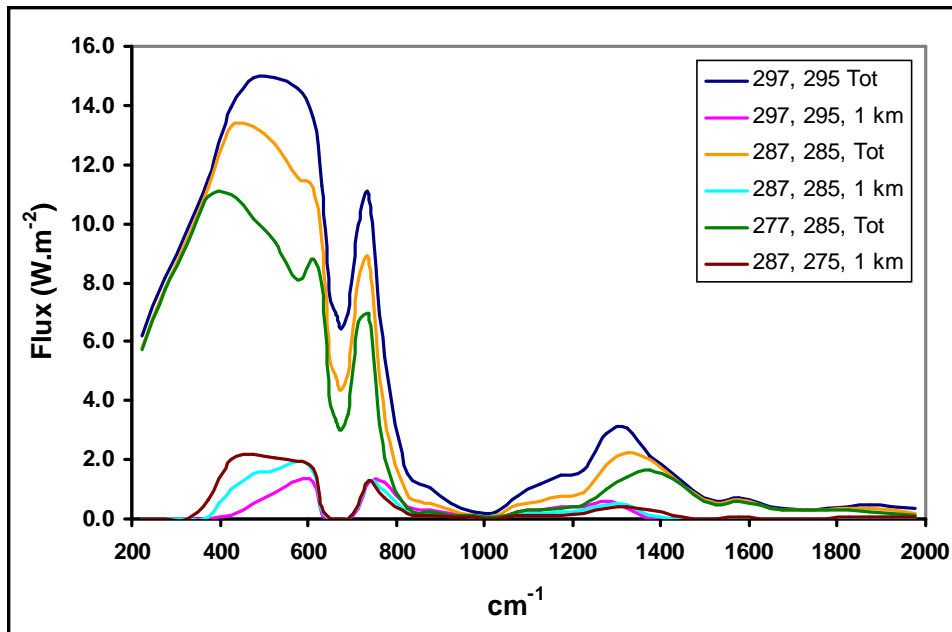


Figure 33: Total upward atmospheric flux and the flux from first 1 km near the surface, 50% RH for the surface, air temperature combinations shown.

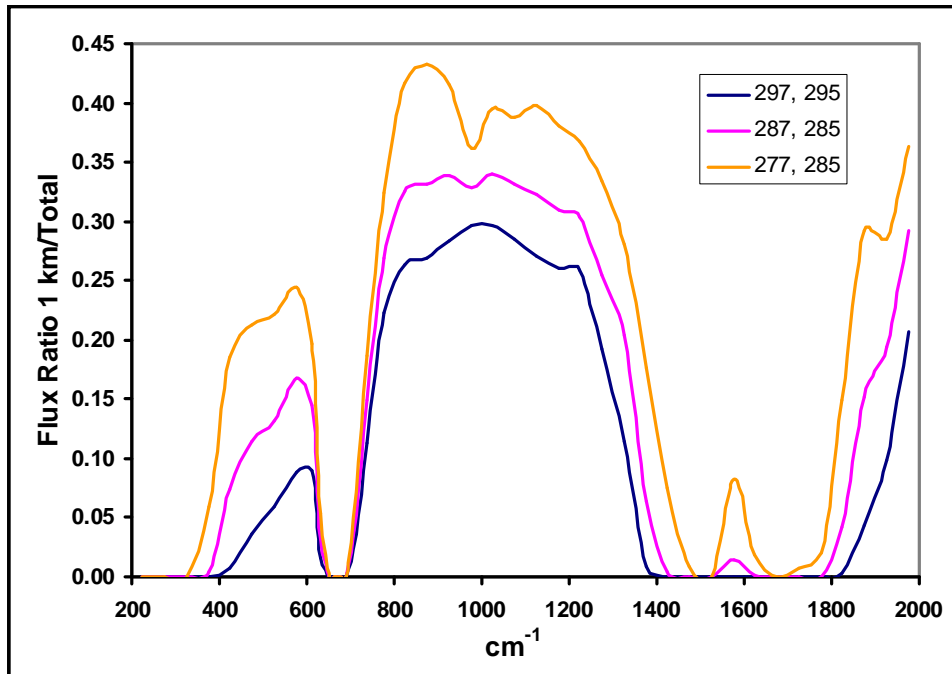


Figure 34: Ratio of the flux from the first km to the total, from Figure 33.

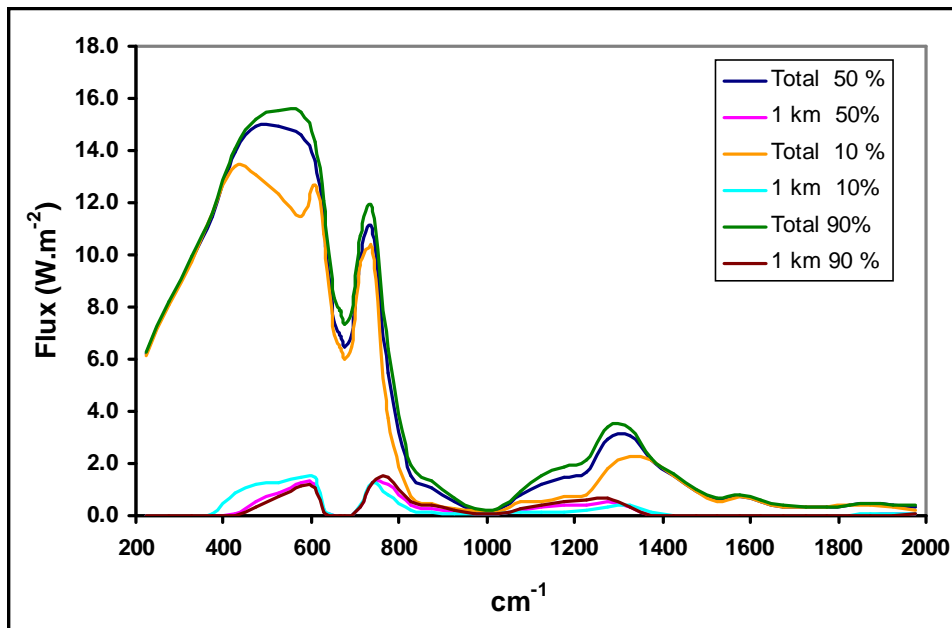


Figure 35: Total upward atmospheric flux and the flux from first 1 km near the surface: 297, 295 K surface, air temperature, RH as shown.

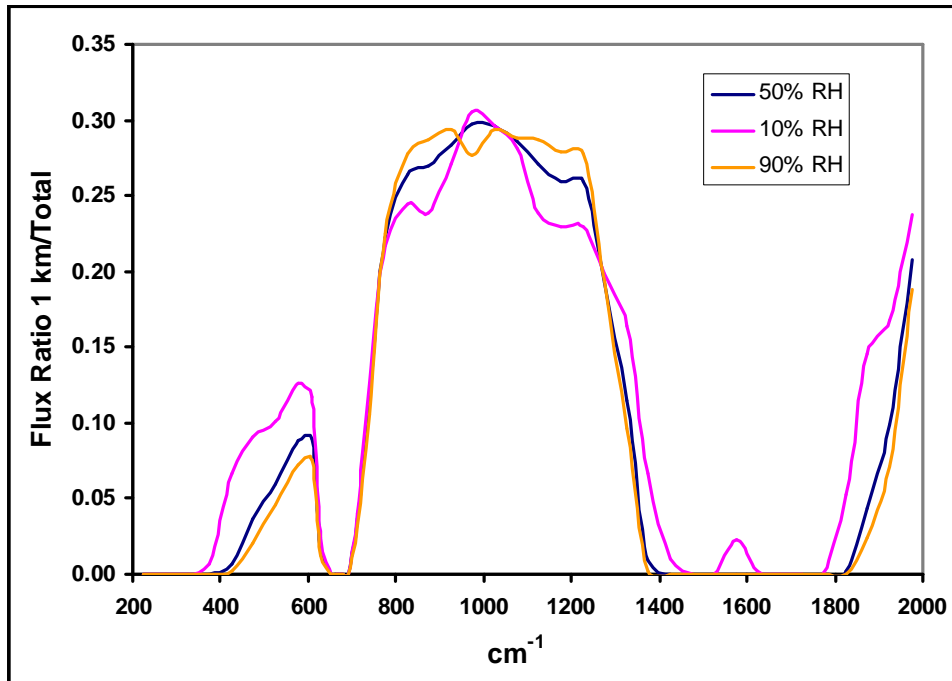


Figure 36: Ratio of the flux from the first km to the total, from Figure 35.

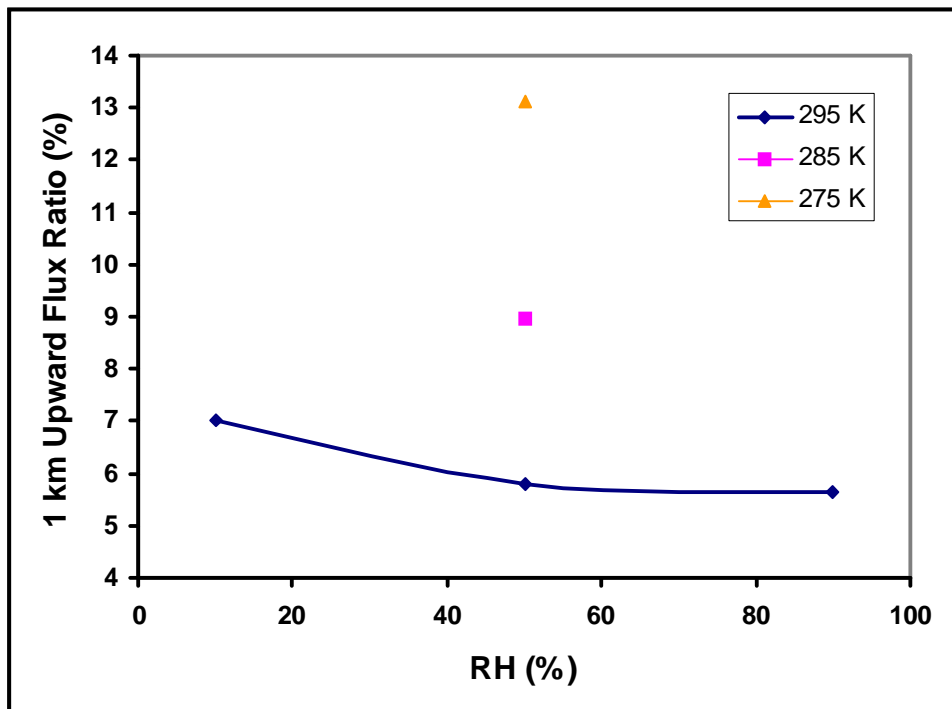


Figure 37: Ratio (%) of 1 km to total upward flux for temperatures and RH shown.

6.1 Atmospheric Cooling Through LWIR Emission

While convection controls the transport of thermal energy up through the troposphere, the Earth can only cool to outer space through the emission of LWIR radiation. As the atmosphere cools with altitude, less of the LWIR flux is absorbed and re-emitted by the IR active molecules because of the decrease in number density and linewidth. For CO₂ and other permanent IR active gases, the concentration decrease is determined by the change in overall air density as the temperature and pressure decrease. However, for H₂O there is also a very large decrease in concentration because of condensation and the decrease in vapor pressure with temperature. The absorption and re-emission of LWIR radiation decreases with altitude and the upward LWIR flux needs to be divided into an ‘exchange’ flux that is reabsorbed and a ‘free photon’ flux that is not. As the linewidth profiles decrease with altitude, the IR photons emitted from the wings of the molecular lines are not reabsorbed at higher altitudes. This is illustrated above in Figure 18. The differences in the line spacing and line profiles between H₂O and CO₂ mean that H₂O is much more effective at cooling the atmosphere than CO₂. Figure 38 shows part of the CO₂ absorption in the P branch of the ν_3 transition between 640 and 660 cm⁻¹. The line profiles at 300 K and 1 atm. at the surface and at 232 K and 0.28 atm. at an altitude of 10 km are shown for 100 m path lengths. At both altitudes, the line centers are saturated. The line broadening coefficients are in the range of 0.06 to 0.08 cm⁻¹.atm⁻¹ and the line spacing of the main P branch lines is approximately 1.5 cm⁻¹. At low altitudes, the adjacent overtone lines are not resolved and the absorption does not decrease much below 0.5 over the spectral range shown. At 10 km, the adjacent overtone lines are partially resolved, but the main P branch lines are not fully separated.

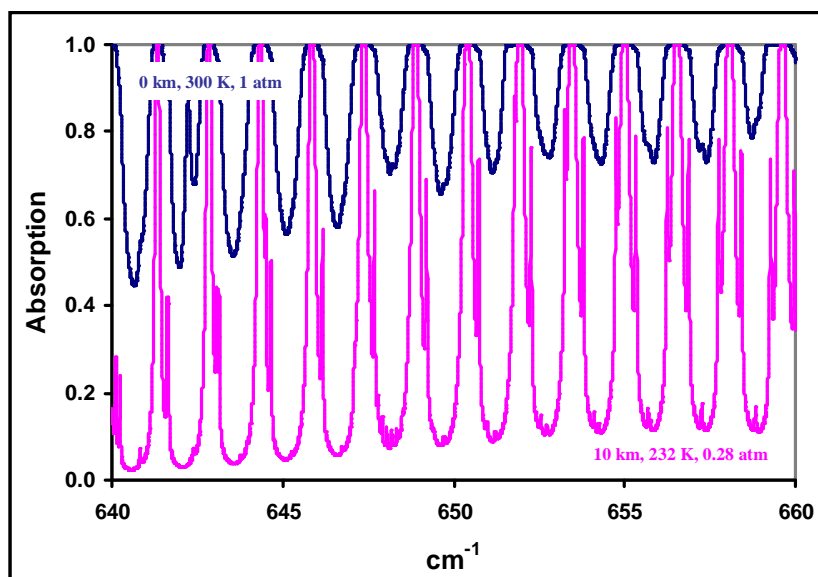


Figure 38: Change in linewidth with altitude in the CO₂ P branch absorption lines of the ν_3 transition between 640 and 660 cm⁻¹.

Figure 39 shows part of the H₂O rotational absorption band between 420 and 440 cm⁻¹. The line profiles at 300 K and 1 atm. at the surface, at 272 K and 0.52 atm. at an altitude of 5 km and at 232 K and 0.28 atm. at an altitude of 10 km are shown for a 100 m path length. The decrease in

linewidth with increasing altitude is much more pronounced. Some of the lines, such as the one near 429 cm^{-1} also show less pressure broadening. The distributions of the pressure broadening coefficients for the H_2O and CO_2 lines used in the radiative transfer calculations are shown in Figure 40. The total number lines for the two species was almost the same, 1361 for H_2O and 1358 for CO_2 , but the linewidths for CO_2 were almost all within the 0.6 to $0.8\text{ cm}^{-1}/\text{atm}^{-1}$ range. Those for H_2O showed a wider range, with almost 40% of the lines having a pressure broadening coefficient below the $0.06\text{ cm}^{-1}/\text{atm}^{-1}$ range.

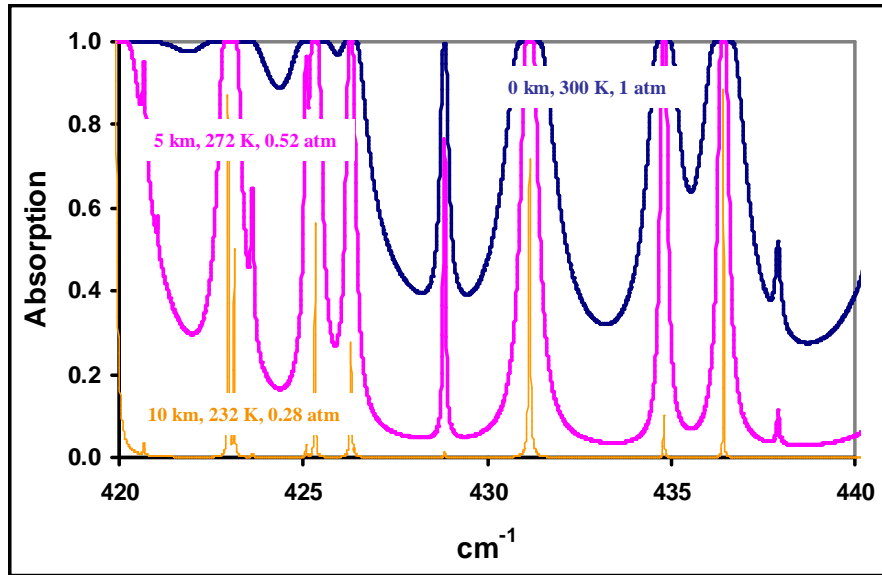


Figure 39: Change in linewidth with altitude in the H_2O absorption lines of the rotational transition between 420 and 440 cm^{-1} .

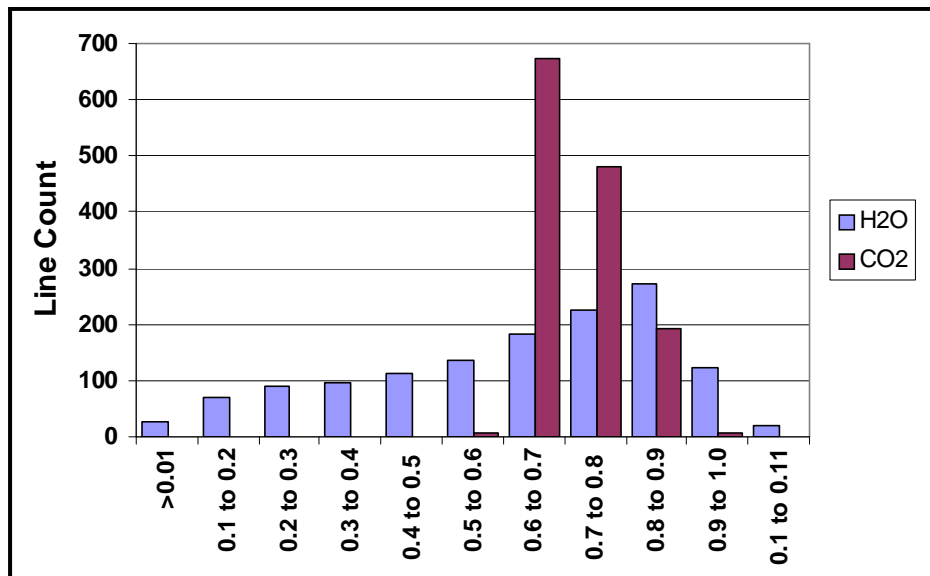


Figure 40: Distribution of the air broadening coefficients of the H_2O and CO_2 lines used in the radiative transfer calculations.

Figure 41 shows the approximate absorptions for H₂O and CO₂ within the first 500 m of the surface for an air temperature of 295 K and an RH of 50%. The surface temperatures vary from 330 to 297 K. The spectral ranges used to estimate the approximate CO₂ and H₂O contributions are the same as for Figure 24 above. Some water lines are included in the CO₂ spectra region. Most of the excess LWIR emission from the surface is absorbed within the first 100 m of the ground. Figure 42 shows the absorption up to 9 km in the atmosphere for the cases shown in Figure 41 with an enlarged absorption scale. The negative absorption above 1 km indicates net LWIR emission and therefore cooling. There is a ‘spike’ near 1.7 km which marks the transition of the lapse rate from -6.5K.km^{-1} to the saturated lapse rate. This produces a minor discontinuity in the radiative transfer model. The H₂O absorption lines show a peak cooling rate near 6 km of $\sim 1.5\text{ W.m}^{-2}$. The peak cooling rate for the CO₂ lines occurs near 4 km at $\sim 0.5\text{ W.m}^{-2}$. From 1 to 9 km, the total cumulative H₂O cooling rate was over 2.5 larger than that of CO₂ at all surface temperatures.

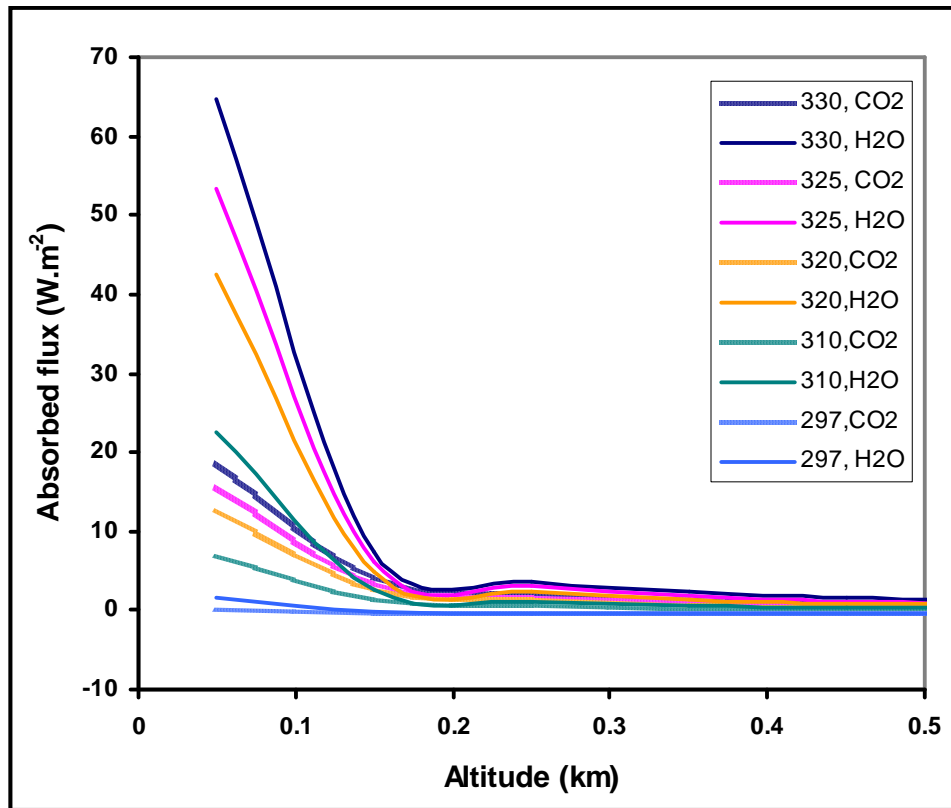


Figure 41: Absorption of surface LWIR emission up to 0.5 km by CO₂ and H₂O for the surface temperatures shown. The air temperature was set to 295 K at an RH of 50%.

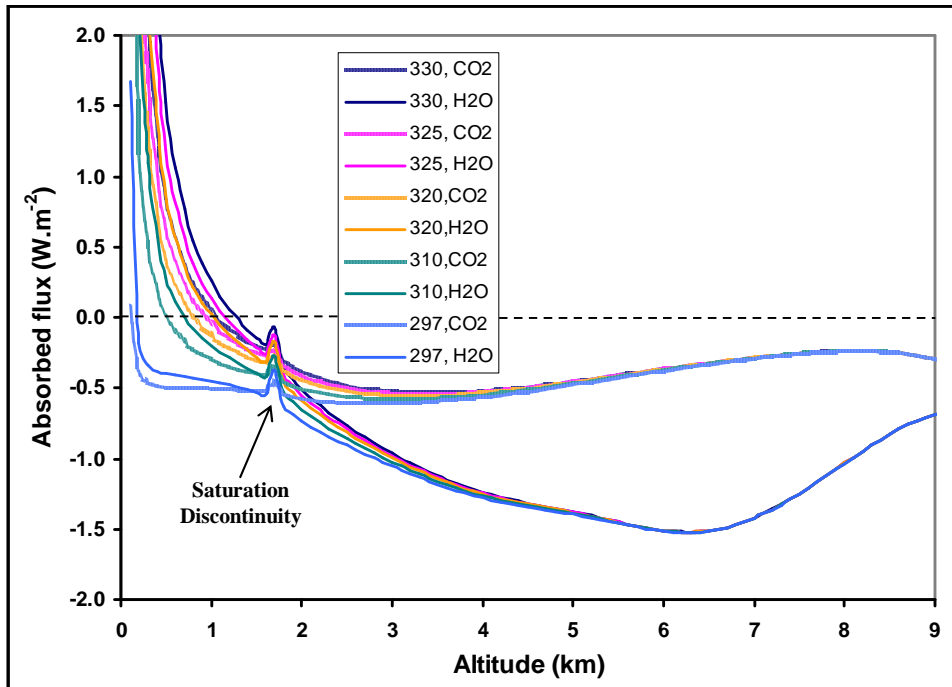


Figure 42: LWIR absorption and emission up to 9 km by CO₂ and H₂O for the surface temperatures shown. The air temperature was set to 295 K at an RH of 50%.

Figure 43 shows a similar plot to Figure 42 for a surface/air temperature of 325/295 K with changes in RH from 90 to 10 %. Except for the lowest RH of 10%, the curves are similar to those in Figure 42. The saturation ‘spikes’ occur at slightly different altitudes, but the cooling rates are similar. At 10% RH, the lapse rate did not transition to the saturated curve until the altitude was 5 km. The 90% RH curve for H₂O shows a higher cooling rate at altitudes above 7 km. The change in cooling rates with RH for the CO₂ curves occurs in part because there are still some H₂O lines in the 550 to 800 cm⁻¹ spectral region used to define the CO₂ absorption. The cooling rates for H₂O are still 2.5 to 3 times larger than for CO₂.

Figure 44 shows a similar plot to Figure 42 for surface/air temperatures of 297/295 K, 287/285 K and 277/275 K with the RH set to 50 %. The maximum cooling rates for H₂O shift to lower altitudes as the surface and air temperatures decrease, but the curve shapes are similar. The emission profiles are shifted to lower altitudes.

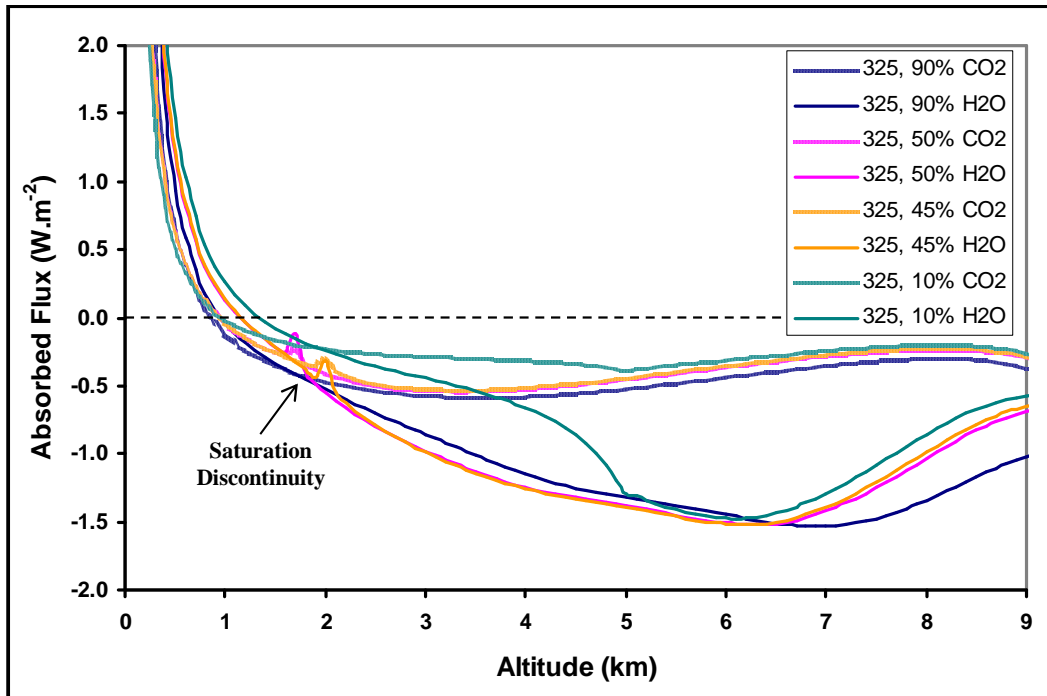


Figure 43: LWIR absorption and emission up to 9 km by CO₂ and H₂O for the RH shown. The surface/air temperatures were set to 325/295 K. The changes in the CO₂ emission rates with RH are from residual water lines in the same spectral region.

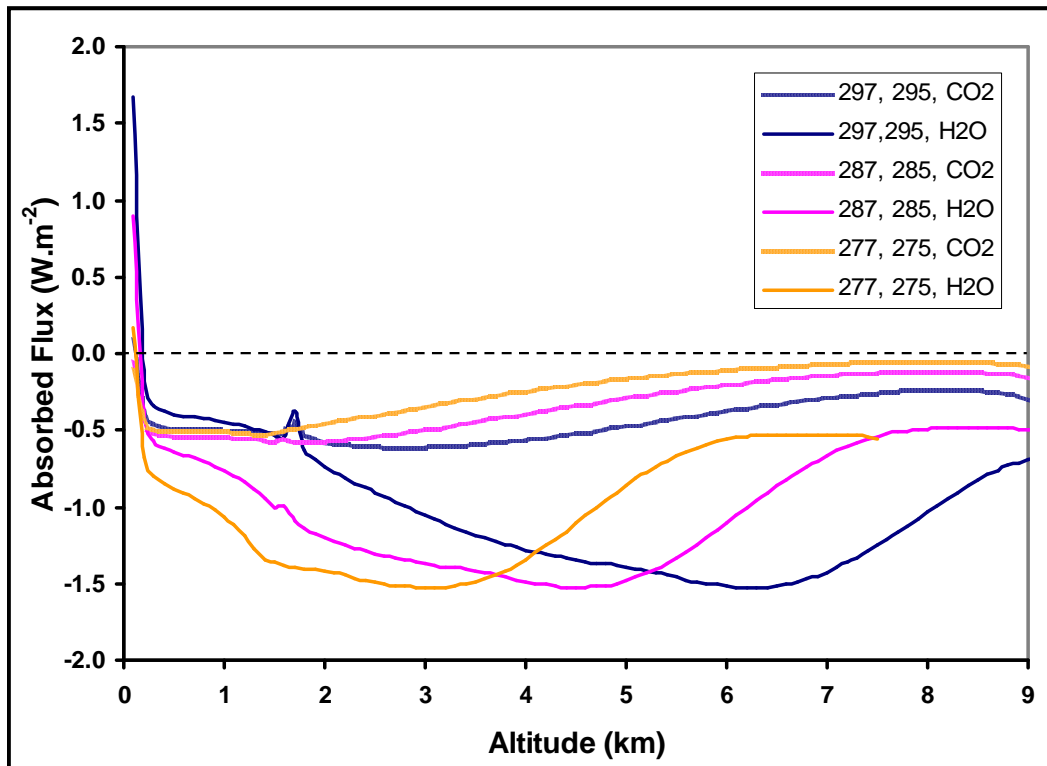


Figure 44: LWIR absorption and emission up to 9 km by CO₂ and H₂O for the surface/air temperatures combinations shown. The RH was 50% in all cases.

Figure 45 shows the effect of changes in the CO₂ concentration from 200 to 500 ppm on the CO₂ contribution to the atmospheric LWIR cooling. Four cases are shown with surface, air temperatures of 325, 295 K; 297, 295 K; 287, 285 K and 277, 275 K. The RH is 50% in all cases. Four CO₂ concentrations, 200, 280, 380 and 500 ppm are shown for each case. For each surface and air temperature combination, the cooling magnitude decreases slightly as the CO₂ concentration is increased. This is the opposite of the cooling changes with concentration for H₂O. However, these changes are too small to have a measurable effect on the overall LWIR cooling rate of the atmosphere.

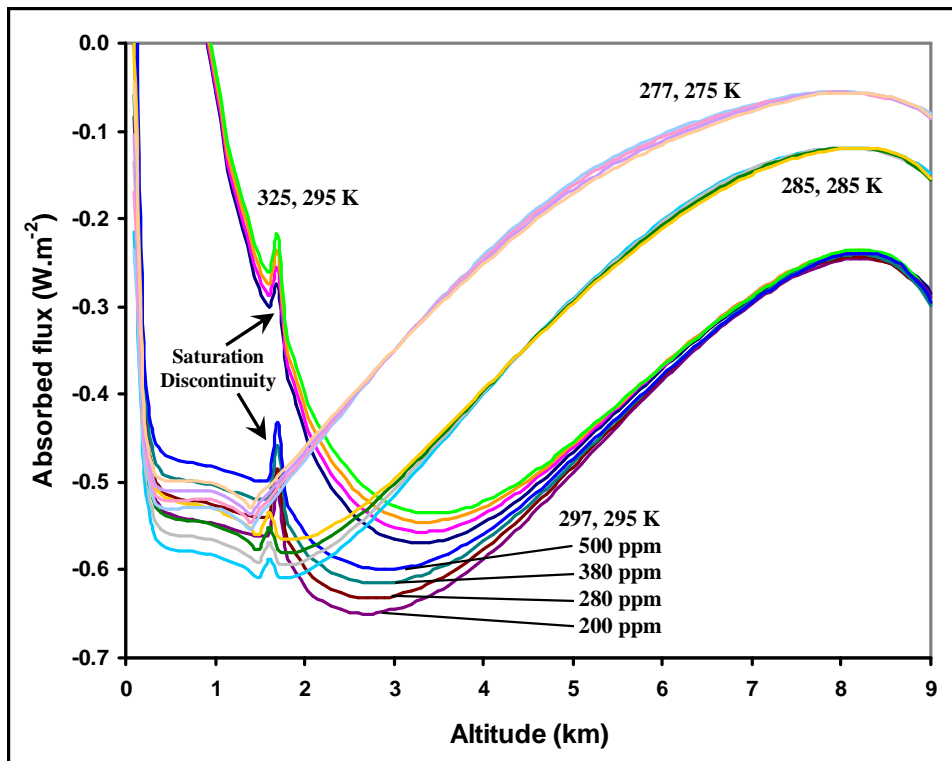


Figure 45: Change in the CO₂ contribution to the LWIR cooling when the CO₂ concentration is changed from 200 to 500 ppm. Surface and air temperatures are shown on the plots. The RH is 50% in all cases.

7.0 Conclusions

The energy transfer processes that set the Earth's surface temperature are more complex than the simple 'equilibrium thermal blanket' greenhouse effect usually described in the literature. There is indeed a 'thermal blanket', but this is simply the downward LWIR emission that originates mainly from the first kilometer layer of air above the surface. However, the temperature of this layer is reset on a daily basis by the local weather conditions and the surface convection. It does not control the surface temperature. This is set by the dynamic balance of the short term energy flux coupled to the surface. There is no thermal equilibrium at the surface. When the 1.7 W.m⁻² increase in downward 'clear sky' LWIR flux from a 100 ppm increase in atmospheric CO₂ concentration is added to the daily flux variations that may exceed 1100 W.m⁻² it becomes clear

that this can have no effect on surface temperature. Similarly, the meteorological surface air temperature (MSAT) is the temperature measured in an enclosure placed at eye level, 1.5 to 2 m above the ground. The MSAT also cannot be changed by an increase in atmospheric CO₂ concentration of 100 ppm. The observed 'global warming signal' is just the effect of ocean surface temperatures on the MSAT.^[19]

The concept that energy transport through the troposphere is controlled by radiative transfer is also incorrect. Thermal energy is transported upwards through the atmosphere by convection. This is a mass transport process. As the air mass ascends through the atmosphere it must overcome the gravitational potential pulling it downwards towards the surface. This is the origin of the air cooling with altitude that produces the atmospheric temperature profile or lapse rate. This cooling is set by the bulk thermodynamic properties of the moist air during the ascent and the turbulent mixing with the surrounding air. Small changes in CO₂ concentration have no effect on this process. As the moist air rises and cools with altitude, the latent heat released by water condensation adds to the convection. The local atmospheric temperature profile is reset on a daily basis by the convective energy 'pulse' that ascends from the surface.

As the pressure decreases with altitude, the molecular linewidths become narrower. In quantum mechanical terms, this is a consequence of the Heisenberg Uncertainty Principle applied to the decrease in the molecular collision frequency. The pressure decrease in turn is controlled by the gravitational potential. As the molecular lines become narrower with increasing altitude, the LWIR radiation emitted by the wings of the pressure broadened lines at lower altitudes is no longer re-absorbed at the higher altitudes. This produces the transition from Kirchoff exchange to a free LWIR flux that emerges at the top of the atmosphere. Because of the decrease in H₂O concentration with altitude resulting from condensation and the decrease in vapor pressure, H₂O, not CO₂ controls the free photon flux that is emitted from the troposphere. The IR active molecules in the atmosphere will always emit LWIR radiation to space. The dynamic balance between the upward convection, the downward mixing and the LWIR emission determines the limit to which air can rise through the troposphere. This dynamic interaction sets the height of the tropopause.

The so called 'greenhouse effect' temperature difference between the average surface temperature and the effective atmospheric average emission temperature of 33 K is determined by convection and the lapse rate. It is a measure of the thermal gradient at the surface produced by the daily solar heating. There is no 'average equilibrium surface temperature' of 288 K. The surface equilibrium temperature that would be produced by a surface solar flux of 1000 W.m⁻² is ~364K. It is the dissipation of this surface flux through the atmosphere by convection that determines the temperature profile near the surface. These energy transfer processes are controlled by gravity not by LWIR photons. This is illustrated in Figure 46

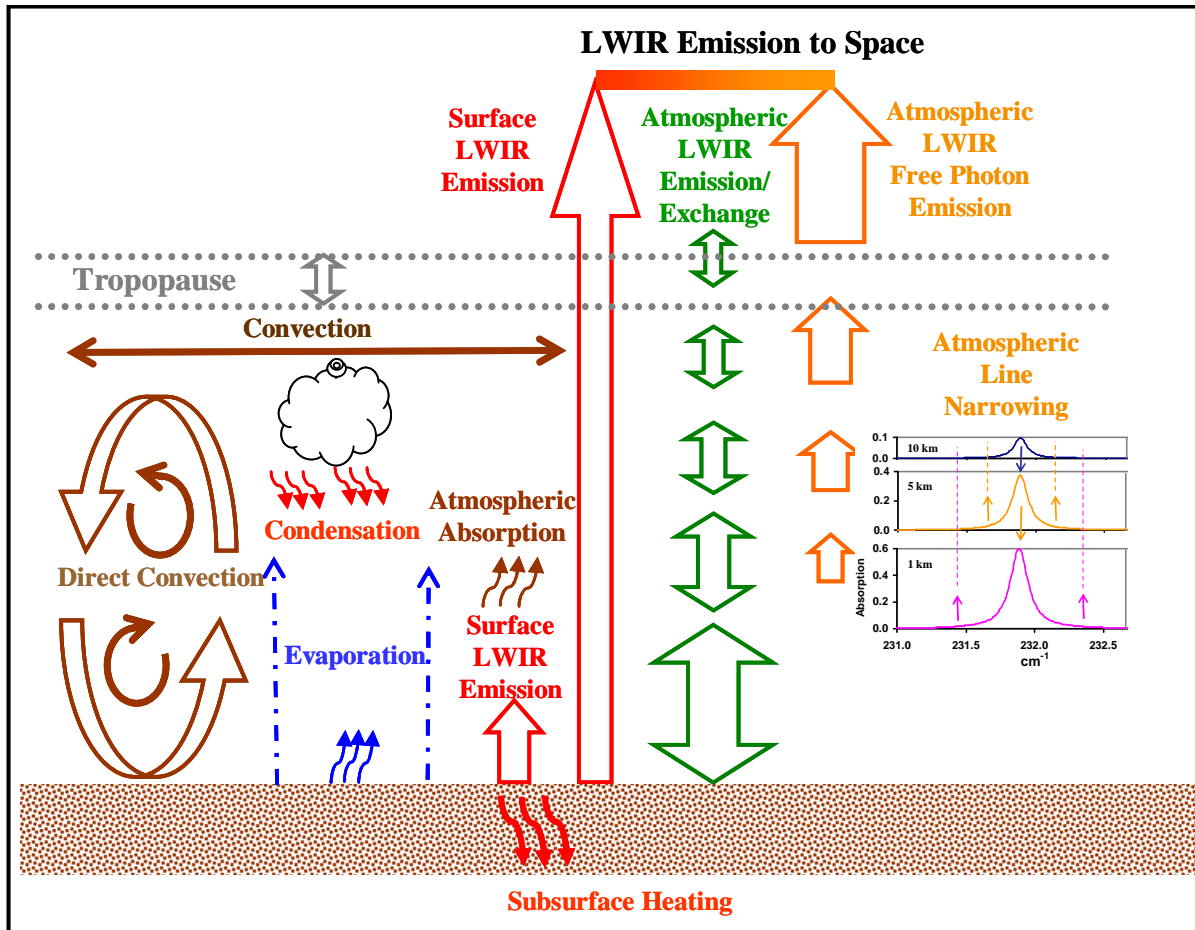


Figure 46: Energy transfer through the atmosphere from the air-land interface: (schematic).

References

1. Fourier, B. J. B., *Mem. R. Sci. Inst.* **7** 527-604 (1827), 'Memoire sur les temperatures du globe terrestre et des espaces planetaires'
2. Tyndall, J., *Proc. Roy. Inst.* Jan 23 pp 200-206 (1863), 'On radiation through the Earth's atmosphere'
3. Agassiz, L. *Etudes sur les Glaciers*, Neuchatel, Paris, (1840).
4. Arrhenius, S. *Philosophical Transactions* **41** 237-276 (1896) 'On the influence of carbonic acid in the air upon the temperature of the ground'
5. Callendar, G. S., *J. Royal Met. Soc.* **64** 223-240 (1938), 'The artificial production of carbon dioxide and its influence on temperature'
6. Revelle, R. and H. E. Suess, *Tellus* **9**: 18-27 (1957), 'Carbon dioxide exchange between atmosphere and ocean and the question of an increase of atmospheric CO₂ during the past decades'
7. Clark, R., *Energy and Environment* **21**(4) 171-200 (2010), 'A null hypothesis for CO₂'
8. Taylor, F. W. *Elementary Climate Physics*, Oxford University Press, Oxford, 2006. [Chapter 7.]
9. Rothman, L. S. et al, (30 authors), *J. Quant. Spectrosc. Rad. Trans.* **96** 139-205 (2005), 'The HITRAN 2004 molecular spectroscopic database'

10. Yu, L., Jin, X. and Weller R. A., *OAFlux Project Technical Report* (OA-2008-01) Jan 2008, 'Multidecade Global Flux Datasets from the Objectively Analyzed Air-sea Fluxes (OAFlux) Project: Latent and Sensible Heat Fluxes, Ocean Evaporation, and Related Surface Meteorological Variables'
11. <http://floats.pmel.noaa.gov/index.html>, *Argo Profiling CTD Floats*, NOAA Pacific Marine Environmental Laboratory.
12. Hale, G. M. and Querry, M. R., *Applied Optics* **12** 555-563 (1973), 'Optical constants of water in the 200 nm to 200 μ m region'
13. Yu, L., *J. Climate* **20**(21) 5376-5390 (2007), 'Global variations in oceanic evaporation (1958-2005): The role of the changing wind speed'
14. Loehle, C. and Huston, J., *Energy and Environment* **19**(1) 93-100 (2008), 'Correction to: A 2000 year global temperature reconstruction based on non-tree ring proxies'
15. <http://sohowww.nascom.nasa.gov/data/data.html>. VIRGO: Near Real Time Data
16. Varadi, F., B. Runnegar, B. and Ghil, M., *Astrophys. J.*, **562** 620-630 (2003), 'Successive refinements in long term integrations of planetary orbits'
17. Zachos, J.; M. Pagani, L. Sloan, E. Thomas and K. Billups, *Science* **292** 686-693 (2001), 'Trends, rhythms and aberrations in the geological climate 65 Ma to present'
18. Oke T. R., WMO/TD-No. 1250, '*Initial guidance to obtain representative meteorological observations at urban sites*', World Meteorological Association, 2006
19. This is based on June 30 2008 data from the 'Grasslands' Ameriflux site. See R. Clark 'What surface temperature is your model really predicting?' Hide the Decline for further details.
20. Weast, R. C., *CRC Rubber Handbook*, 60th edn, CRC Press, Boca Raton, Fl, 1979
21. NASA, *U. S. Standard Atmosphere*, NASA-TM-X-74335, 1976
22. Messiah, A., *Quantum Mechanics*, Dover Publications, Mineola, NY, 1999, Chapter IV, §10